CMOS-MEMS Resonant Gate Transistor-Based Devices

by

Olzhas Tazabekov

A thesis

presented to the University of Waterloo

in fulfillment of the

thesis requirement for the degree of

Master of Applied Science

in

Electrical and Computer Engineering

Waterloo, Ontario, Canada, 2015

AUTHOR'S DECLARATION

I hereby declare that I am the sole author of this thesis. This is a true copy of the thesis, including any required final revisions, as accepted by my examiners.

I understand that my thesis may be made electronically available to the public.

Abstract

The development of the semiconductor industry in general and IC (Integrated Circuits) fabrication technologies in particular enabled the miniaturization of moving electro-mechanical structures down to micrometer size. This significantly reduced the cost and power consumption, and improved the performance of modern Micro-Electro-Mechanical Systems (MEMS). Electrostatically-driven MEMS-based resonators are used in a vast range of applications, including sensors, high frequency filters, time reference signal generations, etc. However, with the resonance frequency continuously increasing and the physical dimensions of the resonators shrinking, the sensitivity of capacitive detection is becoming a major problem due to decreased output signals. The Resonating Suspended Gate Field Effect Transistor (RSG-FET) is seen as a perfect solution to overcome this problem. It replaces conventional capacitive detection with FET detection when the vibrating gate modulates the channel current.

This thesis presents an RSG-FET-based resonator fabricated using conventional CMOS technology with additional post-processing. The concept of RSG-FET combines the advantages of both a high mechanical quality factor and an intrinsic gain of a transistor. The physical mechanisms behind the operation principle along with its advantages and disadvantages are thoroughly investigated using distributed and lumped analysis as well as Finite Element Analysis (FEA) methods. Various approaches for tuning the resonance frequency are studied analytically and verified experimentally.

The fabrication of the device is carried out through a post-processing of a conventional CMOS process (TSMC CMOSP35). Possible applications for RSG-FET-based devices in high frequency filters and atomic force microscopy are also investigated.

Acknowledgements

I would like to express my sincere gratitude to Professor Raafat R. Mansour for being my supervisor and giving me the chance to be involved in his research group. His wisdom, encouragement, support and attention, from beginning to end, made this research a wonderful journey. It is an honor to be his student.

As well, I extend heartfelt thanks to my colleagues and the CIRFE group members for their invaluable support and help during the past few years. Special thanks also go to our lab manager, Bill Jolley, for taking care of the complicated assemblies I needed for my measurements.

Dedication

This thesis is dedicated to my beloved parents, Aislu Zhumabayevna and Khazikan Kaidarbekovich. All I have and will accomplish is only possible because of their love and sacrifices.

Table of Contents

List of Figures

LIST OF TABLES

Chapter 1

MEMS (Micro-Electro-Mechanical Systems) technologies have become firmly established within high-volume commercial markets all over the world. MEMS devices can be found nearly everywhere, such as in inertial sensors/accelerometers (e.g., car airbags, smart phones, gaming accessories), ink-jet printer nozzles, projection displays, microphones, and disk-drive read/write heads. Moreover, radio frequency (RF) MEMS have been moving out of laboratories and into commercial products, offering a better performance over conventional solid-state electronic devices and helping to implement advancements within a broad range of applications, from smart sensor networks to RF components (filters, oscillators, etc) and the Internet of Things.

The development of the semiconductor industry in general and IC (Integrated Circuit) fabrication technologies in particular enabled the miniaturization of MEMS down to micrometer size. This significantly reduced both the cost and power consumption while also improving the performance of MEMS devices. Modern commercial MEMS devices (e.g., MEMS transducers and actuators) are fabricated with technologies compatible to those of IC components. They can carry control electronics onboard, thereby reducing signal noise and enhancing sensitivity, and making “smart” sensors even smarter.

As a result of the commercial success of the first MEMS devices, a new generation of MEMS became prevalent research topics in a wide range of applications. Among these devices, MEMS resonators are the most promising in terms of size, mass, Q-factor and IC-compatibility. The resonators can be used in numerous applications, such as in communications (where they can become a solution for time reference signals and filtering applications) and in sensors (where the resonant frequency is directly or indirectly changed when environmental factors vary, e.g., temperature, light, mass, etc.).

1.1 Motivations

Electrostatic actuation was introduced over four decades ago and has found numerous applications in actuation and sensing. Modern electrostatic (i.e., capacitive) resonators require submicron or even deep submicron electrode-to-resonator gaps in order to alleviate electro-mechanical coupling, reduce motional impedance, increase resonant frequency, and lower actuation voltage, all of which is critical for reasonable actuating performance and IC compatibility [1]. The sizes of the gaps are limited by MEMS fabrication technology. However, with fabrication technology approaching nanometer sizes and MEMS resonators likewise shrinking, the sensitivity of capacitive detection is becoming a major problem due to decreasing output signals.

In view of the above limitations, an RSG-FET (Resonant Suspended Gate Field Effect Transistor) is seen as the ideal solution for overcoming these problems. It replaces conventional capacitive detection with FET detection when the vibrating gate modulates the channel current. This allows the output signal of the resonator to be enhanced thanks to the inherent transconductance gain of FET. Moreover, FET detection allows for the decreasing of electrostatic MEMS actuation voltage, which makes the resonator compatible with modern low-voltage CMOS fabrication processes by decreasing production costs as well as power consumption [2].

The first RSG-FET device was introduced over 60 years ago [3]. Modern fabrication processes (e.g., CMOS) gave a boost to the concept and brought new MEMS functionality into solid-state MOS transistors [4]. RSG-FET consists of a gate suspended over the oxide/semiconductor channel by supporting anchors. By applying a voltage to the gate, one forms a MOSFET inversion layer and creates an electro-mechanical force, which causes a vertical deflection of the mechanical gate and drain current modulation. A non-equilibrium state occurs between electric and elastic forces at a value

slightly larger than 1/3 of the gap (similar to conventional electrostatic MEMS) because of the internal gate potential.

The concept of RSG-FET can be utilized to design a new generation of MEMS devices in a broad range of applications such as microelectronics (memory components) [5], power management (sleep and stand-by transistors) [6], automotive industry (accelerometers, gyroscopes) [7], sensors (pH, magnetic, temperature, humidity sensors) [8], communications (oscillators, filters), characterization tools (MEMS atomic force microscopes [AFM, ultrasound transducers for 2D/3D positioning]), and other smart components (microphones, speakers). Using commercially available foundry-oriented CMOS processes with some additional post-processing enables one to batch-fabricate arrays of SG-FET-based MEMS with active control electronics onboard, which is a significant advantage in terms of reliability and cost.

Even though SG-FET MEMS resonators bring many advantages, these do not come for free. The downscaled devices suffer from all forms of damping (e.g., media damping, anchor damping, thermal damping, etc.), which affects their Q factor. On top of that, there is noise coming from the MOSFET device, which directly affects the sensitivity of the device.

Overall, combining an RSG-FET resonator with proper excitation techniques would lead to a new generation of MEMS resonators with a vast range of applications, especially sensors, Atomic Force Microscopy (AFM) probes, and RF components for communications.

1.2 Objectives

The objective of this research is to design, build, and test a chip-scale CMOS MEMS RSG-FET resonator for applications in sensors, AFM, and RF filters. The major tasks are:

1) Exploring the advantages and disadvantages of RSG-FET and the physical phenomena behind its operating principle, including: a) a distributed, lumped and FEA analysis of an RSG-FET-based resonator; and b) possible approaches for resonance frequency tuning, tunability range, and improving the resonator quality factor.

A thorough understanding of the RSG-FET-based resonator operation principle is key to designing efficient, robust and reliable MEMS devices. Good tunability range is crucial for applications like high-frequency filters and reference signal generators. Moreover, the Q factor is one of the most important properties of MEMS resonators as the devices become smaller, especially if they are used to build sensors based on resonant frequency change monitoring. Generally speaking, the higher the value of Q, the better the microsystem performance is.

One way of achieving a high Q is to decrease the damping (e.g., operate the microsystem in a vacuum). Another way is to use parametric excitation, which consists of modulating the structure's stiffness coefficient at a harmonic frequency of the device's natural resonant frequency. This should improve the frequency response of the device and make it more robust to noise and resistive to damping, thus leading to better sensitivity and performance.

2) Designing, fabricating and characterizing an RSG-FET-based CMOS-MEMS resonator, including: a) designing RSG-FET for maximum efficiency using conventional foundry-oriented CMOS process; b) post-CMOS release processing using in-house clean room facility; and c) characterization and testing of the fabricated RSG-FET-based CMOS-MEMS resonators.

The development of CMOS fabrication technologies enabled the miniaturization of moving electro-mechanical structures down to micrometer size, significantly reducing the cost and power consumption while improving the performance of MEMS devices. However, in order to build efficient and reliable MEMS-based sensors, one needs to interface them with analog electronics. This is usually done through either the discrete or integrated approach. The successful integration of microsystems and active circuits on a single silicon chip is still a bottle-neck of the modern MEMS industry, and most of the recent RSG-FET devices were fabricated using in-house facilities. Exploiting a commercially available CMOS process with additional post-processing aims to address that issue, which would lead to a severe reduction of parasitic signals and production costs.

1.3 Thesis Outline

Following the motivations and objectives stated above, a comprehensive literature survey on electrostatically driven CMOS MEMS RSG-FET is presented in this work.

Chapter 2 presents a brief history of Resonant Gate Transistor-based Micro-Electro-Mechanical systems, which starts with the research of H.C. Nathanson and R. A. Wickstrom. Their work gave birth to a new generation of devices, which were later called microsystems. Modern fabrication technologies gave a boost to these kinds of devices. The chapter also covers the device principles of operation, current state-of-the-art in design and fabrication, and existing operation methods and applications.

Chapter 3 contains guidelines for MEMS designs based on the lumped and distributed analytical analysis and equivalent models. These guidelines are followed by necessary FEM simulations. The dependence of resonator parameters (resonance frequency, coupling efficiency, motional resistance, etc.) on the physical dimensions of the resonator is extensively analyzed. Theoretical aspects of

resonance frequency tuning using DC bias and Joule heating are investigated, as are Q factor and impedance mismatch improvements via the mechanical coupling of several resonators.

Chapter 4 describes the approaches used to fabricate an RSG-FET-based CMOS-MEMS resonator. In order to release the moving mechanical structures, metal and polysilicon layers in the CMOS material stack have been used. The chapter also contains results of characterizations obtained with the laser vibrometer and lock-in amplifier.

Chapter 5 concludes this research.

Chapter 2

2.1 History and State-of-the-Art

In 1965, H.C. Nathanson and R.A. Wickstrom suggested using a passive mechanical resonance to achieve high-Q frequency selectivity in integrated circuits instead of active semiconductor devices with RC feedback, due to their inherent extreme sensitivity of Q to component variations. [8] They made a four-terminal cantilever-like insulated gate-type of transistor exhibiting band-pass properties. The mechanical resonant frequency of this movable cantilever-like gate is the centre frequency of the band-pass device. The work was one of several that gave an initial start to the development of MEMS technology and laid the groundwork for MEMS-based sensors, accelerometers, gyroscopes, microscopes, etc.

The development of modern fabrication technologies allowed for the re-discovery of the Resonating Gate Transistor concept. In 2001, D. Dobrescu and A. Ionescu investigated and modeled the behaviour of the Suspended Gate MOSFET as a voltage programmable switch that could undergo On/Off states due to the pull-in effect in a capacitor with a movable plate [12]. Later, the hysteresis behaviour of the I_D-V_G characteristics of SG-FET for various drain voltages was adopted to design a memory cell. A width of the hysteresis was controlled by the quantity of charges injected in the oxide of the MOSFET. In addition to the snapping, when the device is either On or Off (i.e., the gate is either collapsed or released), the Resonating Gate transistor can operate as a resonator, exploiting advantages of both moving mechanical parts and MOSFET readouts.

N. Abele and A. Ionescu implemented 16 MHz and 91 MHz micromechanical resonators based on Resonant Suspended Gate MOSFET with 750 KHz possible tuning. They showed that the lowest actuation voltage for the MEMS resonator is less than 1 V, which means it can be driven with conventional CMOS circuitry [2]. Oscillators are one possible application for using resonators. A 9.4 MHz micro-electromechanical oscillator based on a tuning fork Vibrating Body FET was implemented [13]. The oscillator has a quality factor of 9400 in the open-loop configuration and low equivalent resistance, which makes it an interesting candidate for a fully integrated oscillator.

More recently, the feasibility of device fabrication and the possibility of integration with modern IC technologies have become as important as device operational characteristics. C. Durand and colleagues developed a 14 MHz in-plane nanomechanical resonator based on SG-FET and discussed its In-IC integration perspectives [14]. They also compared MOS capacitive and MOSFET detection, and showed a 4.3 dB transmission improvement of the latter one. One promising way to build fully integrated Resonant Gate FET-based devices would be using CMOS foundry-oriented fabrication with some additional post-processing steps at an in-house facility. C. Chin and colleagues successfully implemented a CMOS-MEMS Resonant Gate Field Effect Transistor utilizing the 0.35 μm CMOS fabrication process of the Taiwan Semiconductor Manufacturing Company and maskless dry and wet etch post-processing [4]. Their MEMS device shows a Q factor of higher than 1700 and a signal-to-feed-through ratio greater than 40 dB.

Having a thorough understanding of SG-FET operation and an ability to predict its behavior is vital. Since the device can be considered an electrostatic MEMS with MOSFET readout detection, conventional MOSFET analytical models can be incorporated into the analytical models of SG-FET-based devices [15]. For the resonating gate transistor itself, several models have been developed in

order to understand the mechanical motion of the gate and predict the drain current correlated to gate-to-source voltage and drain-to-source bias voltage [16][17][18]. Analysis shows that RG-FET pull-in and pull-out voltages depend on the stiffness and geometry of the suspended gate and are slightly different from the voltages of conventional electrostatic MEMS due to the capacitive divider created by an oxide layer, depletion, and inversion layers.

The correct modeling of a parallel plate electrostatic actuation in capacitive MEMS in general and RG-FET in particular is an important step in designing devices with better operational characteristics, as is an understanding of the devices' actuation principles. Even though the first resonators were driven in direct linear resonance, parameter excitation has been fascinating scientists since the beginning of the 19^{th} century, when Faraday observed that the surface waves of fluid-filled resistors exhibit periodic motion that is twice the vertical excitation frequency. Since then, many studies have observed parametric resonance in structural systems [9]. In the field of MEMS, parametrically excited systems started attracting significant attention due to their distinct advantages of nearly ideal stop-band rejection and an extremely sharp response roll-off, which is important for filtering applications [19]. It has also been shown that parametric excitation can reduce parasitic signals in capacitive sensing [10].

Many groups are currently trying to exploit parametric excitation to develop a new generation of highly sensitive MEMS-based devices (e.g., sensors, accelerometers, filters, AFMs, etc.). Zhang and Turner demonstrated an amplified response mass sensor exploiting a parametric excitation [20]. Rhoads and colleagues proposed an improved band-pass filter, which was composed of tunable comb-drive electrostatic actuators [19], and DeMartini and colleagues investigated the tuning of

effective linear and non-linear stiffness of the oscillator, showing softening and hardening phenomena [21].

2.2 Resonant Suspended Gate Transistor

The concept of Resonant Gate Transistor (RGT) was introduced over 40 years ago and was described as an electrostatically excited tuning fork employing a field-effect transistor readout which permits high Q frequency selection to be incorporated into silicon integrated circuits [22]. RGT consists of three essential elements: 1) an input transducer to convert an input electrical signal into a mechanical force (i.e., electrostatic actuation); 2) a mechanical resonator (i.e., suspended mechanical gate); and 3) an output transducer to sense the motion of the mechanical resonator and generate a corresponding electrical signal (i.e., a field effect transistor current modulation).

The operational principle of RGT is shown in Figure 1. An applied gate voltage creates a combined electro-mechanical force while forming a conductive channel (i.e., accumulation or inversion layer in the channel). The created force moves the suspended gate, which results in an increase of the gate-to-channel capacitance, creating a super-exponential dependence of the inversion charge on the gate voltage in the sub-threshold regime. In other words, the movable part determines the gate capacitance, which defines the threshold voltage [1].

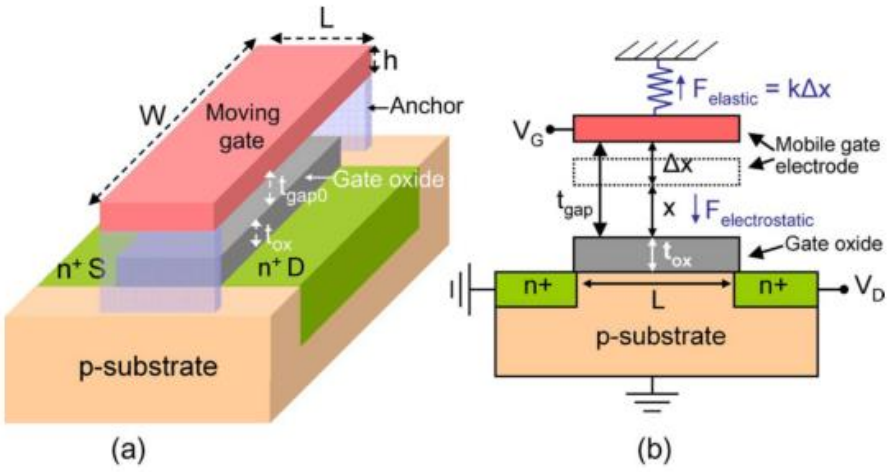

Figure 1 N-channel RGT: (a) 3D structure of RGT with resonating gate suspended over the channel, (b) RGT cross-section [18]

Hence, one may conclude that RGT is a dynamic threshold voltage (V_t) device with a high V_t in the Off state (i.e., low drain current I_d) and a low V_t in the On state (i.e., high drain current I_d).

Like any electrostatically-driven MEMS, RTG also features a mechanical hysteresis, which means that the gate snaps to the substrate at a certain value of the applied voltage and goes back to suspended state at another value. Those voltages are called pull-in (V_{pi}) and pull-out voltages (V_{po}), respectively.

2.2.1 Analysis of Operation

RTG can be considered a combination of capacitances that include an air gap capacitance (C_{gap}), an oxide capacitance (C_{ox}), and a depletion/invertion (C_d, C_{inv}) layer capacitance, which together form a capacitive voltage divider for an externally applied gate voltage (V_G), decreasing an actual MOSFET intrinsic gate voltage (V_{Gint}). One can consider C_{ox}, C_d and C_{inv} as an equivalent intrinsic gate-to-

channel capacitance (C_{gc}) [23]. The resulting equivalent capacitive divider circuit is shown in Figure 2.

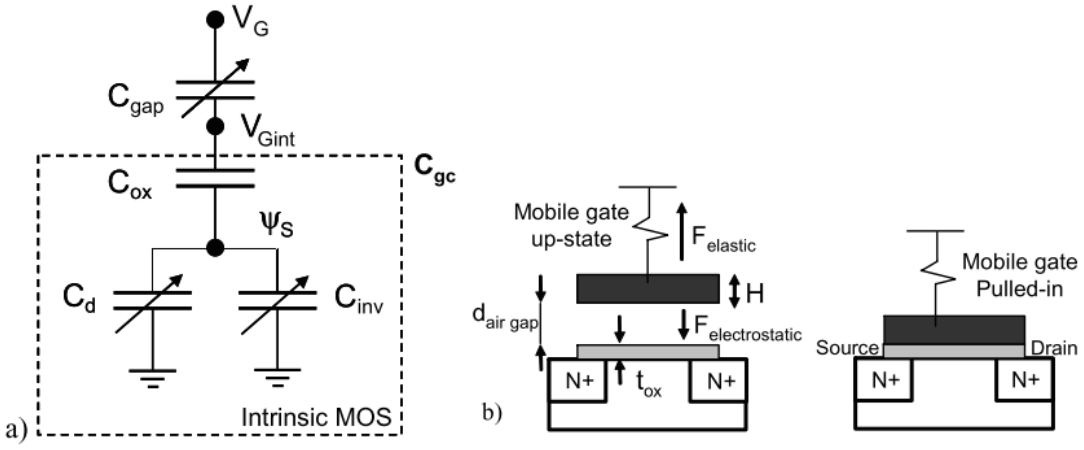

Figure 2 (a) RGT capacitive divider equivalent circuit, (b) RGT pulled-in and pulled-out state [24]

Thus, when V_G is applied to the gate, V_{Gint} is brought down to:

$$V_{Gint} = \frac{V_G}{1 + \frac{C_{gc}}{C_{gap}}} \tag{2-1}$$

The suspended gate moves downwards under the resultant electro-mechanical force (F_R), which is created by the gate voltage and consists of electrostatic and elastic forces.

$$F_R = kx - \frac{1}{2}\frac{\epsilon_{air} A (V_G - V_{Gint})^2}{(t_G - \Delta x)^2} \tag{2-2}$$

where Δx is the gate displacement, k the beam spring constant, t_G the initial gap, ϵ_{air} dielectric constant of the air, and A the area. When V_G is equal to V_{pi}, the system reaches its unstable equilibrium and the suspended gate, which is deflected by Δx, snaps to the substrate. For simple

parallel plate capacitor MEMS, it is shown that the displacement where the snapping occurs is $x_{pi} = \frac{2}{3} t_G$, and that V_{pi} is given by:

$$V_{pi} = \sqrt{\frac{8}{27} \frac{k {t_G}^3}{\epsilon_{air} A}} \tag{2-3}$$

Therefore, MEMS capacitors have a limited tuning range. However, the travel range of the movable electrode could be increased by connecting an additional capacitor C_f in series leading to:

$$x_{pi} = \frac{2 - \frac{C_0}{C_f}}{3} \, t_G \tag{2-4}$$

where C_0 is the minimum gap capacitance. For $\frac{C_0}{C_f} \geq 2$, the instability can be completely eliminated [25].

For an RGT device, the values of V_{pi} and V_{po} are given by:

$$V_{pi} = \sqrt{\frac{8k \left(t_G + \frac{t_{ox}}{\epsilon_r} \right)^3}{27 \, \epsilon_{air} W \, L}}, V_{po} = \sqrt{\frac{2k t_G t_{ox}^2}{\epsilon_{ox} W L}} \tag{2-5}$$

where ϵ_r is the dielectric constant of the gate oxide material, t_{ox} is the gate oxide thickness, and W and L are the transistor width and length, respectively [18].

As can be seen from Figure 1 a, the intrinsic gate-to-channel capacitance can be expressed as [23]:

$$C_{gc} = \frac{C_{ox} C_{inv}}{C_{ox} + C_{inv} + C_d} \tag{2-6}$$

The movable part, in turn, defines the state of the gate capacitance C_{air}, which is either low or high depending on whether it is in On/Off operation mode, which determines the MOSFET threshold voltage. Thus, RGT is a dynamic V_t device via dynamically charged $C_{ox}{}'$, which is a total capacitance of the solid-state and the movable part.

When V_G is applied to a conventional MOSFET, different charges appear across the MOS structure: the gate charge (Q_G) is balanced by the fixed interface charge (Q_{ox}), the inversion layer charge (Q_{inv}) and the depletion charge (Q_{dep}). Thus, the gate voltage (V_G) and the threshold voltage (V_t) are given by:

$$V_G = V_{FB} + \Psi_S + \gamma \sqrt{\Psi_S} - \frac{Q_{inv}}{C_{ox}} \tag{2-7}$$

$$V_t = V_{FB} + \Psi_0 + \gamma \sqrt{\Psi_0} \tag{2-8}$$

where $\gamma = \frac{\sqrt{2q\epsilon_s N_{sub}}}{C_{ox'}}$ is the substrate factor, $\Psi_0 = 2\,\Phi_f + several\,U_t$ is an approximation of the surface potential Ψ_s, ϵ_s silicon dielectric constant, N_{sub} silicon doping concentration [15].

The motional current (I_d), which is related to the charge inversion along the MOSFET channel, is then defined as:

$$I_d = \mu_n \frac{W}{L} \int_{V_S}^{V_D} -Q_{inv}\, dV \tag{2-9}$$

where μ_n is the electron charge mobility.

I. A. 1. Lumped model

A conventional electrostatic MEMS can be modeled as a damped oscillating system using analogies between effective mechanical rigidity (k) and capacitance (C_x), effective mass (m) and inductor (L_x), and damping (γ) and resistance (R_x). The shunt capacitor (C_{gap}) describes the static coupling capacitance between moving and static electrodes (Figure 3). When an AC signal is applied at the frequency equal to the CC beam mechanical resonant frequency, the transfer function is at maximum and the system is in resonance. The resonant frequency can be expressed as:

$$f_0 = \frac{1}{2\,\pi}\sqrt{\frac{k_{eff}}{m_{eff}}} \tag{2-10}$$

The equivalent circuit components can be expressed as functions of the structure's mechanical parameters, applied DC voltage, and beam displacement, as follows [1]:

$$L_x = \frac{m_{eff}}{2\,V_{DC}^2\left(\frac{\partial C}{\partial x}\right)^2} \tag{2-11}$$

$$C_x = \frac{2\,V_{DC}^2\left(\frac{\partial C}{\partial x}\right)^2}{k_{eff}} \tag{2-12}$$

$$R_x = \frac{\omega_0 m_{eff}}{2\,Q\,V_{DC}\frac{\partial C}{\partial x}} = \frac{k_{eff} g_0^4}{\epsilon_0^2 A^2 \omega_0 Q V_{DC}^2} \tag{2-13}$$

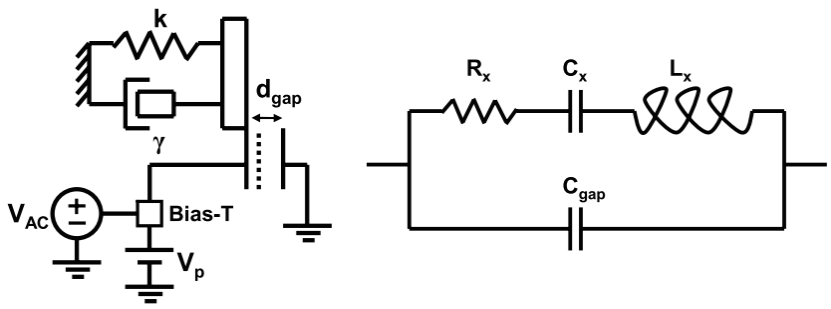

Figure 3 Mechanical and electrical behavioural model of electrostatic MEMS [26]

In order to maximize the resonator Q factor, the value of R_x should be minimized. Also, the C_{gap} should be chosen such that R_x is much smaller than $\frac{1}{\omega\, C_{gap}}$. However, the main reasons for a severe reduction in a resonator's Q factor are gas friction, clamping loss, and surface loss.

RGT can be modeled as an electrostatic MEMS resonator coupled with a small signal model of MOSFET to take into account the transistor gain, as shown in Figure 4.

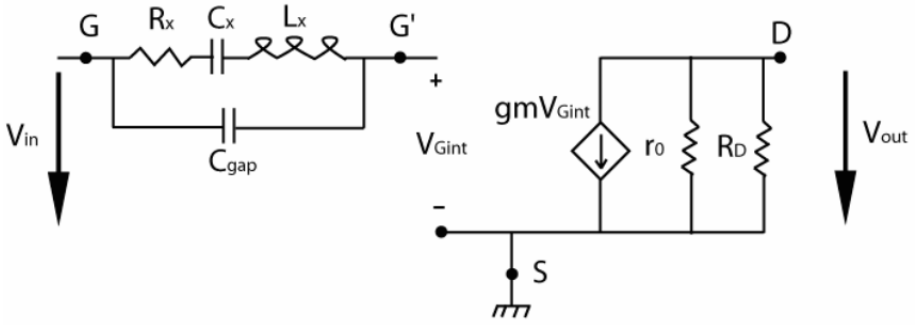

Figure 4 RGT small signal equivalent model [26]

The transfer function of the MOSFET small signal model, taking into account the resistance at the drain (R_D), is given by:

$$\frac{V_{out}}{V_{Gint}} = -g_m(R_D||r_0) \tag{2-14}$$

The total capacitance C_{eq} needed to calculate frequency response is given by:

$$C_{eq} = C_{GS} + C_{GD}(1 + g_m(R_D||r_0)) \tag{2-15}$$

where C_{GS} is the gate-to-source capacitance and C_{GD} is the gate-to-drain capacitance.

C_{eq}, together with an input resistance (R_{in}), creates a low-pass filter with a pole (ω_{pole}^{MOSFET}) defined as:

$$\omega_{pole}^{MOSFET} = \frac{1}{C_{eq}\, R_{in}} \tag{2-16}$$

2.3 Actuation in the Presence of Nonlinearities

The dynamic behavior of most systems can be generally studied as nonlinear, unless there are small variations in parameter, in which case a linear behavior can be assumed. However, at the microscale, the strong influence of nonlinearities makes operating in the linear region difficult and less beneficial. There are several sources of nonlinearities in MEMS, which can be due to forcing, damping or stiffness, as shown in Figure 5 [9].

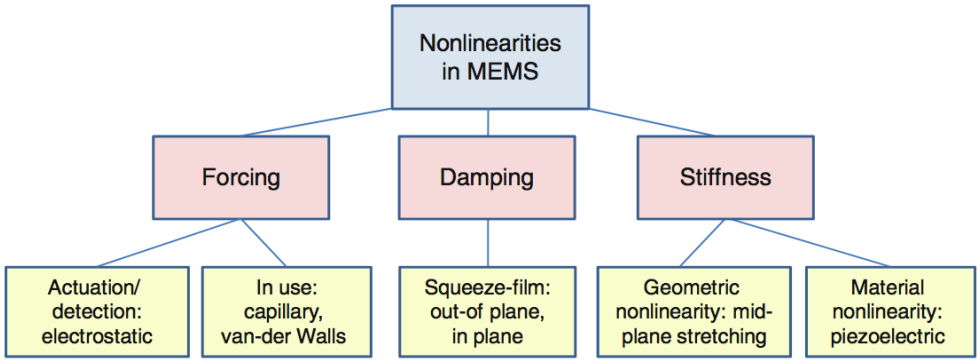

Figure 5 Sources of nonlinearities in MEMS [9]

The influence of nonlinearities on movable structure response when excited by external harmonic forces is a major topic in MEMS. As discussed in [9], resonators can be a framework for many applications such as sensors, probe microscopes and RF filters. In RGT-based devices, the nonlinearities come from both the geometry (CC beam) and the actuation technique (electrostatic forces).

2.3.1 Primary and Secondary Resonances in MEMS

The dynamic response of externally excited structures can be classified into two types: primary and secondary resonances. Primary resonance refers to exciting the structure near its natural resonance frequency, whereas secondary resonance specifies an induction of large motion at frequencies far from the natural resonance.

To understand an influence of nonlinearities, let us consider a case of an electrostatically driven actuator under a DC load, and small AC harmonic perturbation under a viscous damping. The motion equation is given by:

$$m\frac{\partial^2 x}{\partial t^2} + c\frac{\partial x}{\partial t} + kx = \frac{\epsilon A[V_{DC} + V_{AC}\cos(\Omega t)]^2}{2(d-x)^2} \tag{2-17}$$

Assuming that $V_{AC} \ll V_{DC}$ and the displacement consists of a static and dynamic part ($x(t) = u(t) + \delta(t)$), and that expanding the force term in the Taylor series drops the higher order terms, the static equilibrium equation then becomes [9]:

$$\begin{aligned} m\frac{\partial^2 u}{\partial t^2} + c\frac{\partial u}{\partial t} + k_{eff}u + \alpha_q u^2 + \alpha_c u^3 \\ = Fcos(\Omega t) + F_p u\cos(\Omega t) \end{aligned} \tag{2-18}$$

where

$$\begin{aligned} k_{eff} = k - \frac{\epsilon A V_{DC}^2}{(d-\delta^3)}, \alpha_q = -\frac{3\epsilon A V_{DC}^2}{2(d-\delta)^4}, \\ \alpha_c = -\frac{2\epsilon A V_{DC}^2}{(d-\delta^5),}\ F = \frac{V_{DC}V_{AC}}{(d-\delta)^2}, F_p = \frac{2V_{DC}V_{AC}}{(d-\delta)^3} \end{aligned} \tag{2-19}$$

One can notice here the presence of quadratic and cubic nonlinearities and a decrease in the spring coefficient, which has a softening effect on the resonator frequency response. The phenomenon has been found in a broad range of microstructures with different types of actuation.

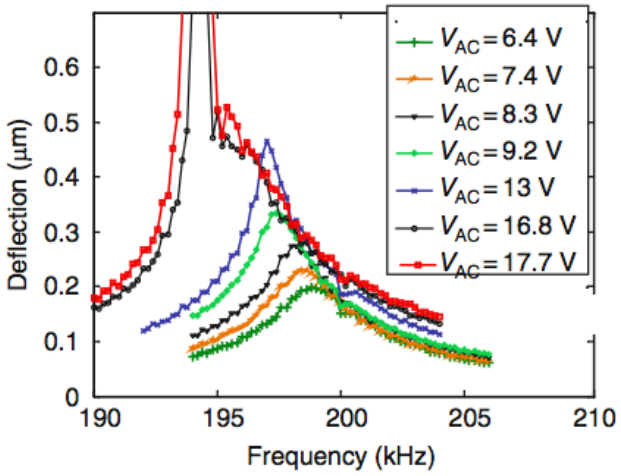

Figure 6 Frequency response of a cantilever micro beam [27]

Figure 6 shows the experimentally acquired data of an electrostatically driven cantilever micro beam frequency response with $V_{DC} = 10\ V$, from which one can observe a softening of a spring coefficient.

2.3.2 Parametric Resonance

Parametric excitation refers to an excitation technique with forces that appear as time-variant coefficients of the differential equation, unlike the external forces described in the previous section. The most significant resonance occurs when the parametric force excitation frequency reaches twice the natural resonance frequency of the system, which is called a principle parametric resonance [9].

Parametric excitation has been extensively studied in MEMS due to its ability to drive microstructures to large distinctive responses easier than in cases of direct excitation, which makes it desirable for many sensing, filtering, and actuation applications.

One can observe the parametric excitation mechanism in an example of double-electrode electrostatic actuation. Assuming the electrodes are placed symmetrically and at the same distance, d, and that the same voltage is applied, ($V_t = V_{DC} + V_{AC}$), the motion equation is given by:

$$m\frac{\partial^2 x}{\partial t^2} + c\frac{\partial x}{\partial t} + kx = \frac{\epsilon A V_t^2}{2}\left[\frac{1}{(d-x)^2} - \frac{1}{(d+x)^2}\right] \tag{2-20}$$

Assuming a small displacement and expanding the resultant electrostatic force in a Taylor series, the equation (2-20) becomes:

$$m\frac{\partial^2 x}{\partial t^2} + c\frac{\partial x}{\partial t} + \left(k - \frac{2\epsilon A V_t^2}{d^3}\right)x - \left(\frac{4\epsilon A V_t^2}{d^5}\right)x^5 = 0 \tag{2-21}$$

One can see that the spring coefficient in the equation varies, representing a parametric force.

A general view of the equation above is called the Mathieu equation and is given as: [9]

$$\frac{d\hat{u}}{d\hat{t}} + \left[\hat{\omega}_n^2 + \hat{f}\cos\left(\hat{\Omega}\hat{t}\right)\right]\hat{u} = 0 \tag{2-22}$$

where $\hat{\omega}_n^2$ is the dimensionless natural frequency, $\hat{\Omega}$ the dimensionless excitation frequency, and $\hat{f}$ the forcing amplitude. The solution of (2-22) is not explicit and is of a complicated form. Floquet analysis established a stability analysis diagram (the Strutt diagram) in terms of the parameters $\omega_n^2 = \frac{4\hat{\omega}_n^2}{\hat{\Omega}^2}$ and $f = \frac{4\hat{f}}{\hat{\Omega}^2}$. The diagram shows shaded zones, called instability tongues, where any pair of ω_n^2, f inside the tongues results in an unstable solution (Figure 7). The largest of these tongues is located at $\omega_n^2 = 1$, which is the principle parametric resonance.

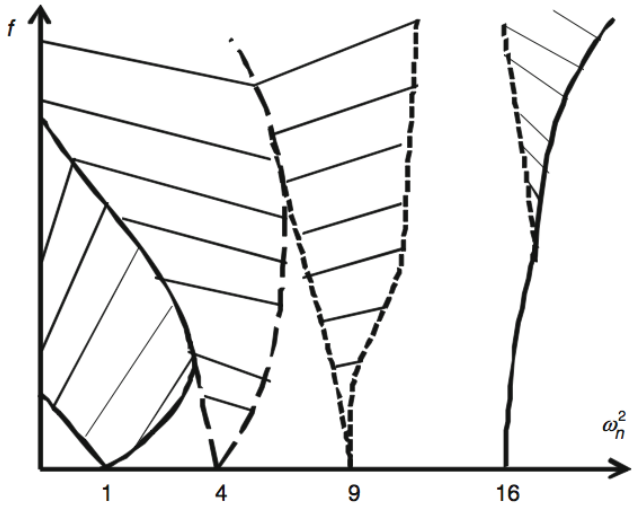

Figure 7 Strutt diagram with instability tongues [9]

2.4 Actuation Using Internal Dielectric Transduction

Internal dielectric transduction is another form of actuation with electrostatic forces that was used to drive bulk acoustic resonators (*FBAR*). This type of transduction has much higher efficiency compared to air-gap electrostatic transduction, which leads to improved electrical performance including lower motional impedance, no pull-in effects, higher Q, and smaller size for higher resonant frequencies [28],[29]. A silicon internal dielectric transduced resonator excited in 3^{rd} and 9^{th} longitudinal harmonics at 1.53 and 4.5 GHz was presented with a Q factor of 1700 and 11200, respectively (Figure 8) [30].

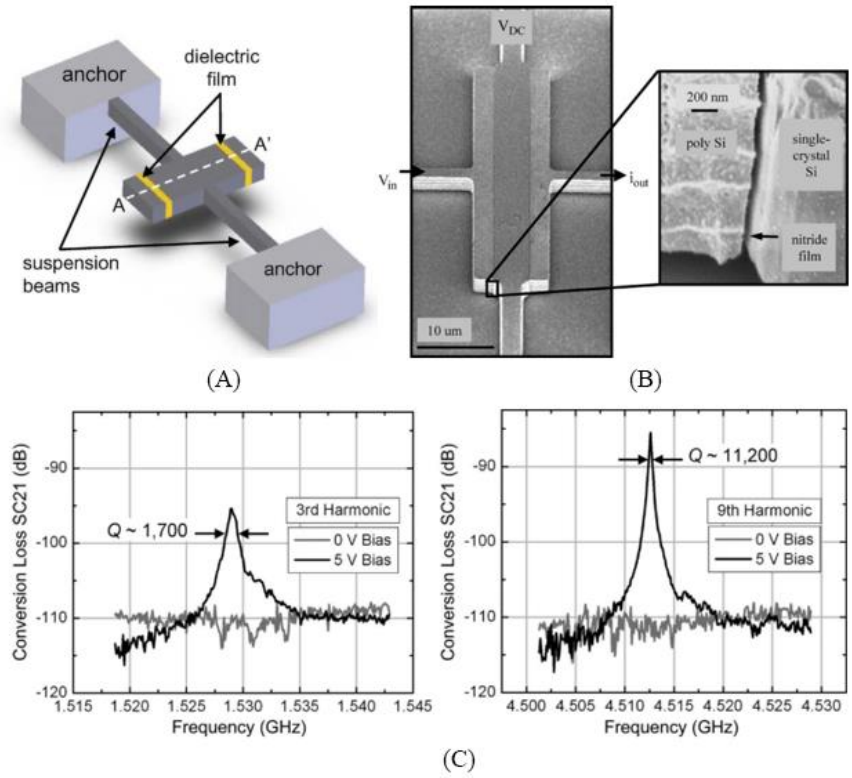

Figure 8 Longitudinal free-free bulk-mode resonators: a) schematics, b) SEM picture, c) measured frequency response of 3rd and 9th harmonics [30]

Internal dielectric transduction was successfully adapted to drive an independent-gate finfet to acoustic resonance [31]. In this configuration, one of the gate's active regions was biased in the accumulation regime to create a large electrostatic force that caused longitudinal vibrations, while another one was biased in the inversion regime, which resulted in a DC channel current. At resonance, elastic waves that formed in the resonator modulated the drain current both by physically changing the gate capacitance and by piezoresistive modulation of the carrier mobility. The fabricated device had a resonant frequency of 37.1 GHz and a Q-factor of 560 [32]. Later on, the unreleased resonant body transistor was successfully implemented. Even though it had a Q factor 4 times lower

than its released counterpart, it still opens up a tremendous opportunity to build high Q, high frequency mechanical resonators that do not require post-processing (Figure 9) [33].

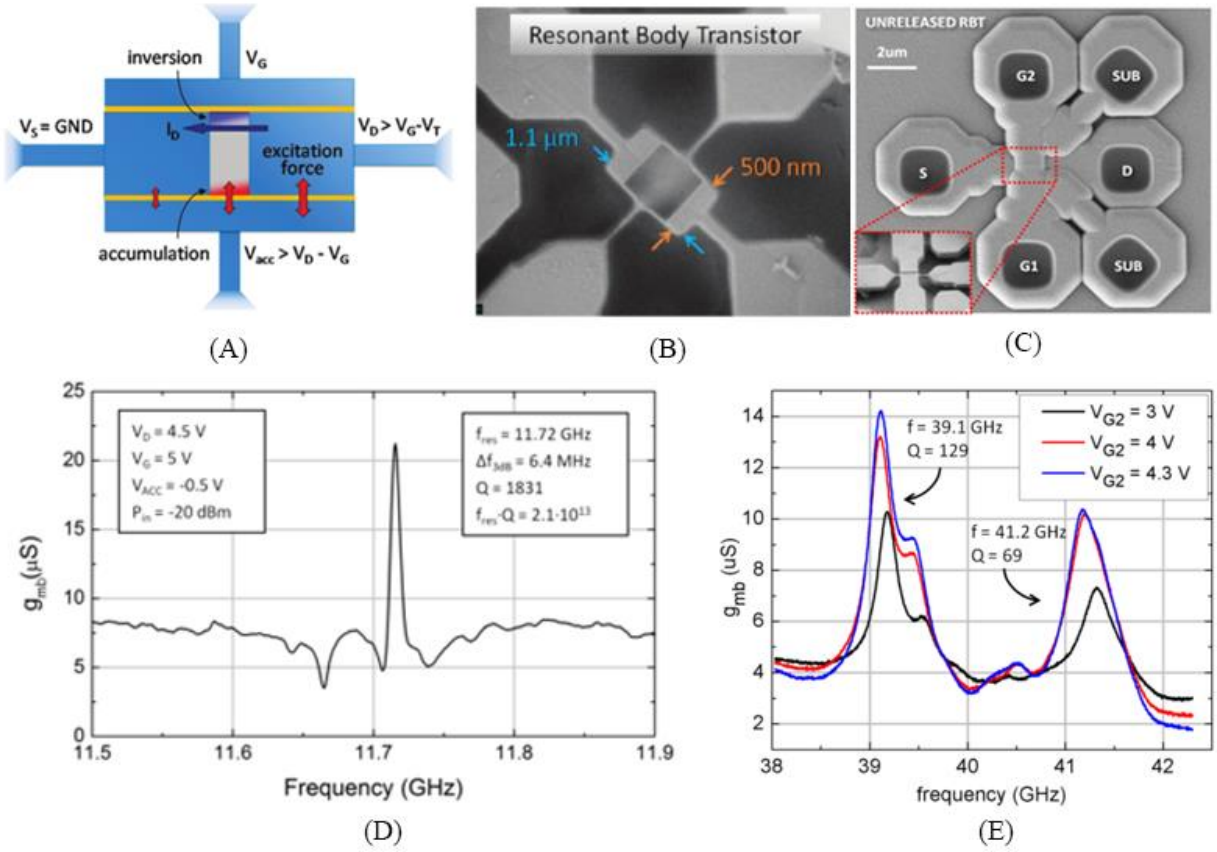

Figure 9 Resonant body transistor: a) schematics, b) SEM picture of released RBT, c) SEM picture of unreleased RBT, d) frequency response of released RBT (f0=11.72 GHz, Q=1831), e) frequency response of unreleased RBT (f0=39.1 GHz, Q=129) [33]

Another type incorporated in a resonator transduction is transduction by depletion forces, which are the forces acting on an immobile charge in the depletion region of a symmetrically doped p-n junction. One of the implemented resonators combined a high Q of air-gap-transduced resonators with the frequency scaling benefits of internally transduced resonators, and exhibited a Q factor of

18000 at 3.72 GHz resonant frequency [34]. A later version of the device had a JFET-based deflection sensing and a Q-factor of 25900 at a 1.6 GHz resonant frequency [35].

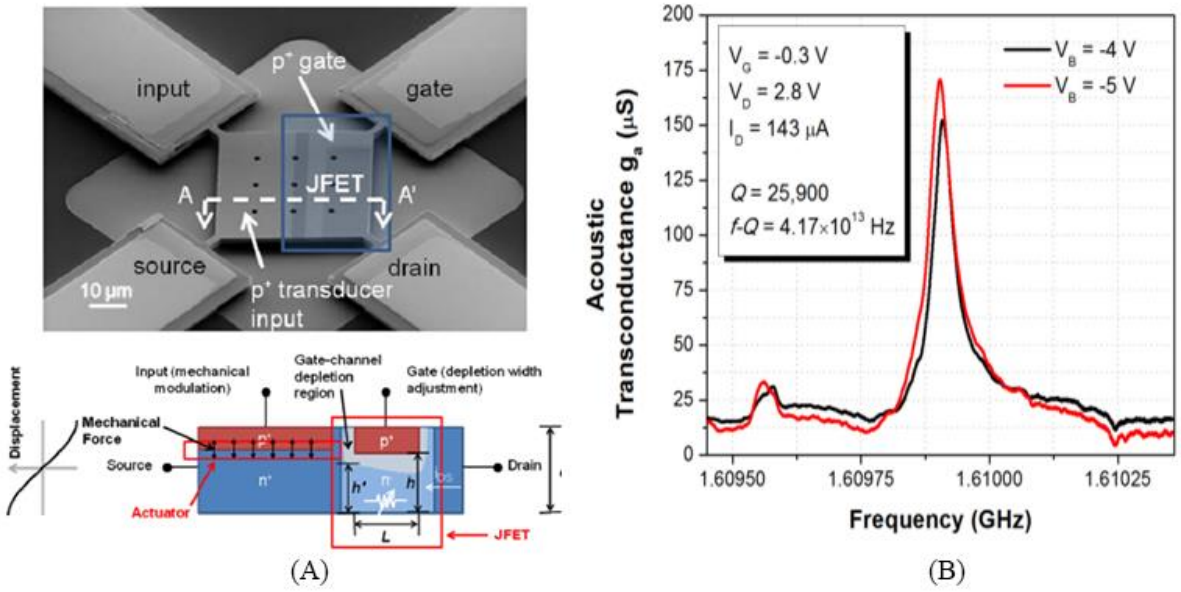

Figure 10 JFET-sensed P-N transduced RF resonator: a) SEM picture and cross- section, b) frequency response (Q = 25000, f0=1.6 GHz) [35]

Considering the above, the frequency scaling capabilities of the internal dielectric transduction method makes it ideal for implementing high frequency RF MEMS resonators. Moreover, they do not have any undesirable features (in this case, pull-in effect) and are resistant to contaminations and generally more robust than their air-gap counterparts. Their ease of fabrication and small size also make this type of resonator quite an attractive replacement for integrated LC elements.

2.5 Chapter Summary

This chapter presented a brief review of the history and current state-of-the-art of the RSG-FET types of MEMS devices, followed by a basic operational analysis, including a description of the physics behind it, simulation models, specifics of actuation, and corresponding issues.

Chapter 3

3.1 Design of RSG-FET-Based MEMS Resonators

RGT MOSFET MEMS resonators are a hybrid of both mechanical and active semiconductor components (i.e., a moving mechanical structure with MOSFET readout). Thus, both parts are designed with extra care to ensure the desired operational features and maximized output during the fabrication step. Moving structures were designed relying on available analytical lumped and distributed models with FEM verification.

3.1.1 Design of Mechanical Part

The design procedure contains three major steps. Step 1 is to refine the desired specifications, such as resonance frequency, tunability range, quality factor, power consumption, signal parameters, etc. The second step is the rough design of the mechanical structures based on the defined specs, material parameters and approximated lumped and distributed analytical models (e.g., Euler-Bernoulli beam theory). FEM analysis with a parametric sweep of the design parameters is the final step to ensure that all the specifications are satisfied.

Several CC beam configurations with different sets of structural materials resonating in the MHz range are reported here. The 1st mode resonance frequency of the beam is given by:

$$f_0 = \frac{\omega_{non}}{2\pi}\sqrt{\frac{EI}{\rho A l^4}}, \tag{3-1}$$

where ω_{non} is a non-dimensional resonant frequency (for CC beams $\omega_{non} = 22.3733$), E is a material Young's modulus, I – moment of inertia, ρ – material density, and A and l are electrode area and resonator length, respectively. Having the geometrical sizes of the resonator defined, one can then calculate the other important parameters, such as pull-in voltage and resonator stiffness.

3.1.2 Finite Element Analysis of CC Beam Resonator

Once the preliminary design is completed, the operational parameters can be verified by FEM software (e.g., COMSOL Multiphysics), which allows for the introduction of minor changes to better meet the desired specifications. Several designed CC beam resonators and their parameters are given in Table 3-1.

Table 3-1. List of Designed CC Beam Resonators with Operational Parameters (Electrostatic Gap $d_0 = 0.2\ \mu m$)

№	Structural materials	Width [um]	Length [um]	Thickness [um]	f_0 (calculated) [Hz]	f_0 (FEM) [Hz]	Pull in (calc) [V]	Pull in (FEM) [V]
1	$SiO_2 + M_1 + SiO_2 + M_4$	5	70	6.515	7.71E+06	7.21E+06	83	89
2	$SiO_2 + M_1 + SiO_2 + M_4$	5	50	6.515	1.51E+07	1.35E+07	162.89	170
3	$SiO_2 + M_1 + SiO_2 + M_4$	5	70	4.59	5.43E+06	5.17E+06	49.1457	54
4	$SiO_2 + M_1 + SiO_2 + M_4$	5	50	4.59	1.06E+07	9.92E+06	96.3255	100
5	$SiO_2 + M_2 + SiO_2$	4.28	6	70	5.06E+06	4.89E+06	253	270
6	$SiO_2 + M_2 + SiO_2$	4.28	4	70	5.06E+06	4.88E+06	253	270
7	$SiO_2 + M_2 + SiO_2$	4.28	6	50	9.93E+06	9.39E+06	496.493	535

The mode shape of one of the designed resonators as well as its maximum static displacement as a function of applied voltage is given in Figure 11.

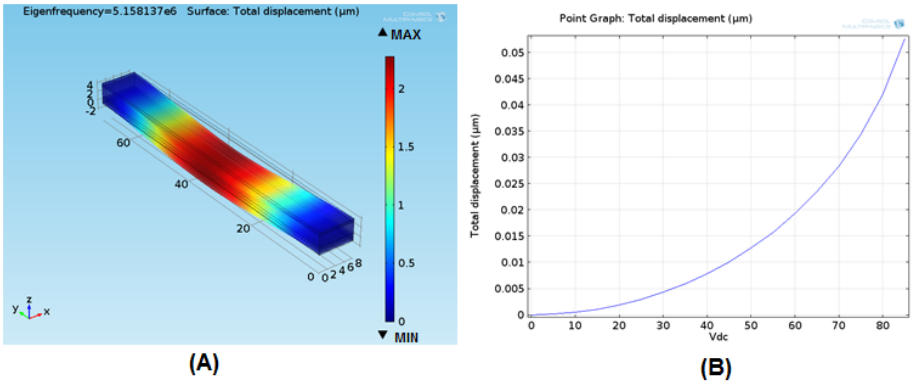

Figure 11 CC Beam electrostatic resonator: a) mode shape, b) maximum static displacement vs. applied voltage

3.1.3 Equivalent Lumped Parameter Mechanical and Electrical Circuits of CC Beam Electrostatic Resonator

For many applications, including the filter design, it is often convenient to define an equivalent lumped-parameter mass-spring-damper mechanical circuit for the resonator. The equivalent mass at location y on the resonator is given by:

$$m_r(y) = \frac{\rho W_r h \int_0^{L_r} [X_{mode}(y')]^2 (dy')}{[X_{mode}(y)]^2} \tag{3-2}$$

The shape mode of the CC beam resonator $X_{mode}(y)$ can be found as:

$$X_{mode}(y) = \zeta(\cos ky - \cosh ky)(\sin ky - \sinh ky), \tag{3-3}$$

$$k = \frac{4.730}{L_r}, \zeta = -1.01781 \; for \; CC \; beams$$

The mechanical stiffness and the damping factor of the resonator are expressed as:

$$k_m(y) = \omega_{nom}^2 \, m_r(y), c_r = \frac{k_m(y)}{\omega_{nom} Q_{nom}} \tag{3-4}$$

where Q_{nom} is the resonator quality factor.

As indicated recently, the resonant frequency of this device can be tuned via adjustment of Vdc. The dependence arises form a V_{dc}-dependent electrical spring constant k_e, which lowers the overall spring stiffness($k_r = k_m - k_e$). The resultant resonance frequency can be expressed as:

$$f_0 = f_0^m \left(1 - \langle \frac{k_e}{k_m} \rangle\right)^{\frac{1}{2}} \tag{3-5}$$

where f_0^m is a mechanical resonant frequency of the beam. The quantity $\langle \frac{k_e}{k_m} \rangle$ now can be found as:

$$\langle \frac{k_e}{k_m} \rangle = \int_{L_{e1}}^{L_{e2}} \frac{dk_e(y')}{k_m(y')} \tag{3-6}$$

where $dk_e(y')$ is the differential electrical stiffness, which depends on the beam-bending shape and gap distance $d(y)$.

$$dk_e(y') = \frac{V_{dc}^2 \, \epsilon_0 \, \epsilon \, b \, dy'}{\left(d(y')\right)^3}, \tag{3-7}$$

$$d(y) = d_0 - \frac{1}{2} V_{dc}^2 \epsilon \epsilon_0 \, b \int_{L_{e1}}^{L_{e2}} \frac{1}{k_m(y')\big(d(y')\big)^2} \frac{X_{mode}(y)}{X_{mode}(y')} \, dy'$$

where d_0 is the initial gap and b is the resonator width.

To conveniently model and simulate the impedance behaviour of the resonators in electromechanical circuits, an equivalent electrical circuit is needed. The electrical equivalent of an electrostatic micro-mechanical resonator consists of a series RLC denoted as motional impedance components, and a shunt capacitor denoted as a feed-through capacitor (Figure 12).

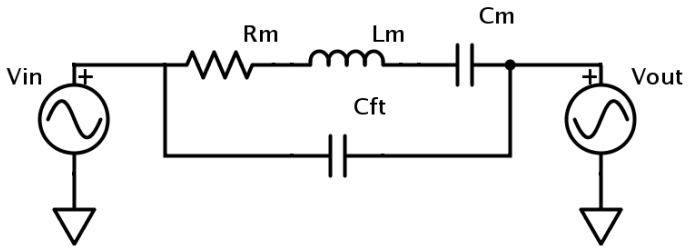

Figure 12 Micro-mechanical resonator equivalent circuit

The values of the motional components can be found as:

$$L_m = \frac{m_{re}}{\eta_e^2}, C_m = \frac{\eta_e^2}{k_{re}}, R_m = \frac{\sqrt{k_{re} m_{re}}}{Q \, \eta_e^2} \tag{3-8}$$

where η_e is an electromechanical coupling factor of the resonator and can be expressed as:

$$\eta_e = \sqrt{\int_{L_{e1}}^{L_{e2}} \int_{L_{e1}}^{L_{e2}} \frac{V_{dc}^2 (\epsilon \epsilon_0 \, b)^2}{\big(d(y')d(y)\big)^2} \frac{k_{re}}{k_r(y')} \frac{X_{mode}(y)}{X_{mode}(y')} dy' dy} \tag{3-9}$$

The value of the electro-mechanical coupling coefficient is very important, as it defines the motional resistance of the resonator which is affected by the resonator Q factor and determines how difficult it would be to integrate and match the resonator into an RF circuit. The following analysis has been carried out to show the influence of the resonator properties on its equivalent circuit components, which would introduce a systematic approach and undoubtedly lead to a better microsystem and built-in electronics design.

Several CC beam configurations have been considered. Their corresponding equivalent circuit parameters have been calculated in Table 3-2.

Table 3-2. CC Beam Resonator Properties and Corresponding Equivalent Electrical Circuit Component Values

№	CC Beam Resonator		Q factor	eta	Lm [H]	Cm [F]	Rm[Ohm]	f0[Hz]
1	**Dimensions [um]:**	$l = 40, h = 2, b = 8,$	3600	8.5×10^{-7}	0.81	2.8×10^{-16}	15×10^{3}	10.6×10^{6}
	Gap [um]:	$d0 = 0.1$	(vac)					
	Biasing [V]:	$V_{dc} = 7[V]$						
	Material Properties	$\rho = 2320\ \left[\frac{kg}{m^3}\right],$	50	8.5×10^{-7}	0.81	2.8×10^{-16}	1.1×10^{6}	10.6×10^{6}
	(Polysilicon):	$E = 160 \times 10^{9}\ [Pa]$	(air)					

2	**Dimensions [um]:** **Gap [um]:** **Biasing [V]:** **Material Properties** **(Aluminum + SiO2):**	$l = 150, h = 3, b = 4,$ $d0 = 0.64$ $V_{dc} = 50[V]$ $\rho = 2200\ \left[\frac{kg}{m^3}\right],$ $E = 70 \times 10^9\ [Pa]$	3600 (vac) 50 (air)	5.5×10^{-7}	5.7	8.5×10^{-14}	2.3×10^3	800×10^3
				5.5×10^{-7}	5.7	8.5×10^{-14}	163×10^3	800×10^3
3	**Dimensions [um]:** **Gap [um]:** **Biasing [V]:** **Material Properties** **(Aluminum + SiO2):**	$l = 70, h = 4.6, b = 5,$ $d0 = 0.1$ $V_{dc} = 30[V]$ $\rho = 2200\ \left[\frac{kg}{m^3}\right],$ $E = 70 \times 10^9\ [Pa]$	3600 (vac) 50 (air)	1.3×10^{-6}	0.8	1.2×10^{-15}	7.1×10^3	5.4×10^6
				1.3×10^{-6}	0.8	1.2×10^{-15}	516×10^3	5.4×10^6

As can be seen from the above, every aspect of the resonator design is important and influences critical parameters. Resonant frequency, coupling coefficient, and motional resistance are of particular interest. Hence, the resonator must be appropriately sized in order to satisfy the desired specifications.

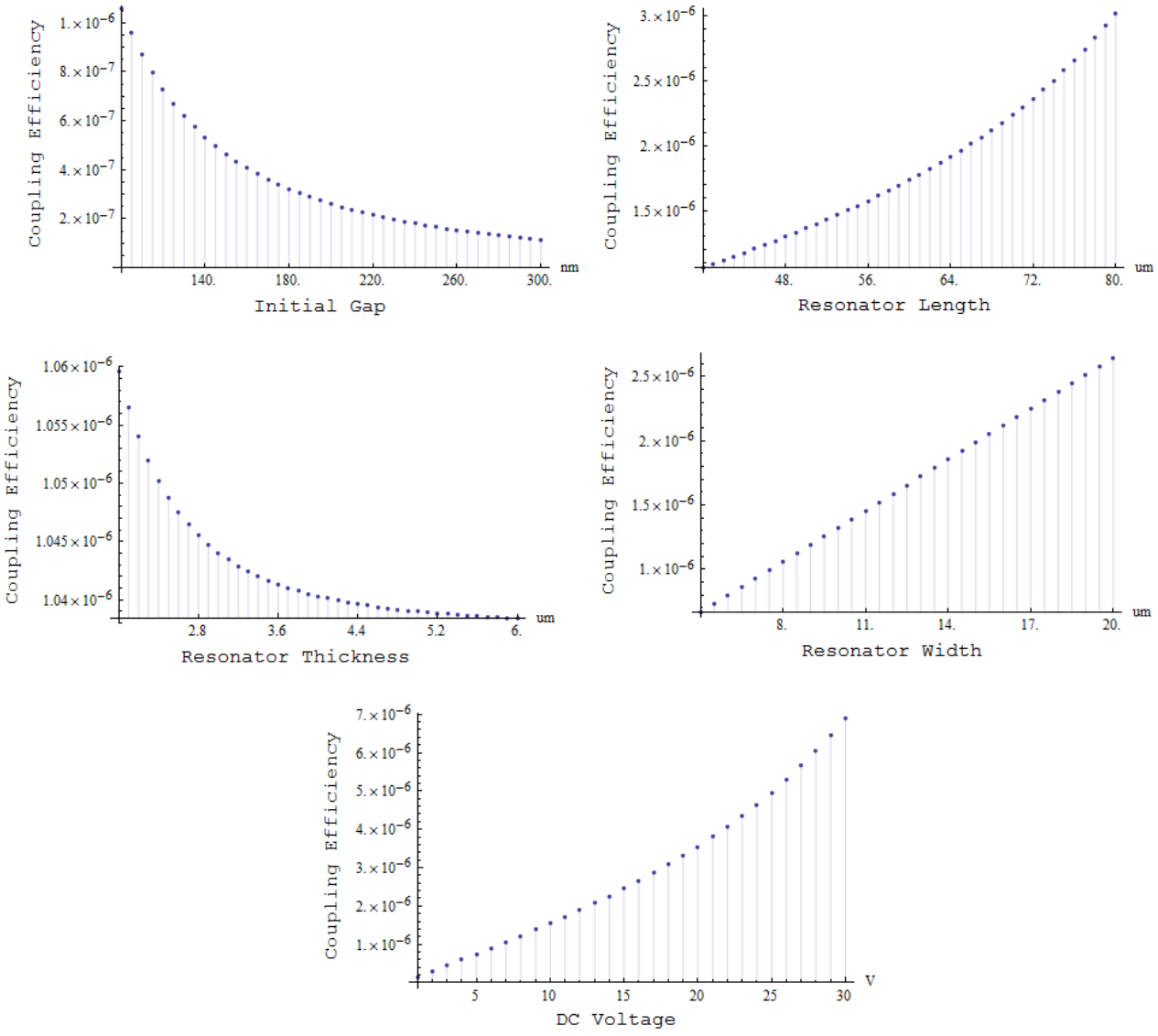

Figure 13 Electro-mechanical coupling coefficient as a function of resonator initial gap, length, thickness, width, and DC bias

For the first CC beam resonator shown in (Table 3-1), Figure 13 shows the dependence of electro-mechanical coupling on the resonator initial gap, length, width and DC bias. One can

notice that increasing width, length and biasing of the resonator improves the coupling, which leads to better performance.

Figure 14 shows that the resonator motional resistance increases with the initial gap and thickness, and decreases with larger length, width and DC bias voltage. One may observe that in order to design mechanical resonators with better performance, one should decrease the resonator electrostatic gap and thickness, as well as increase the beam length and width operating it at higher DC voltage. The resonant frequency of the device changes only slightly with the initial gap or resonator width, but it does increase with the resonator thickness and decrease with increase of both the DC bias and length (Figure 28).

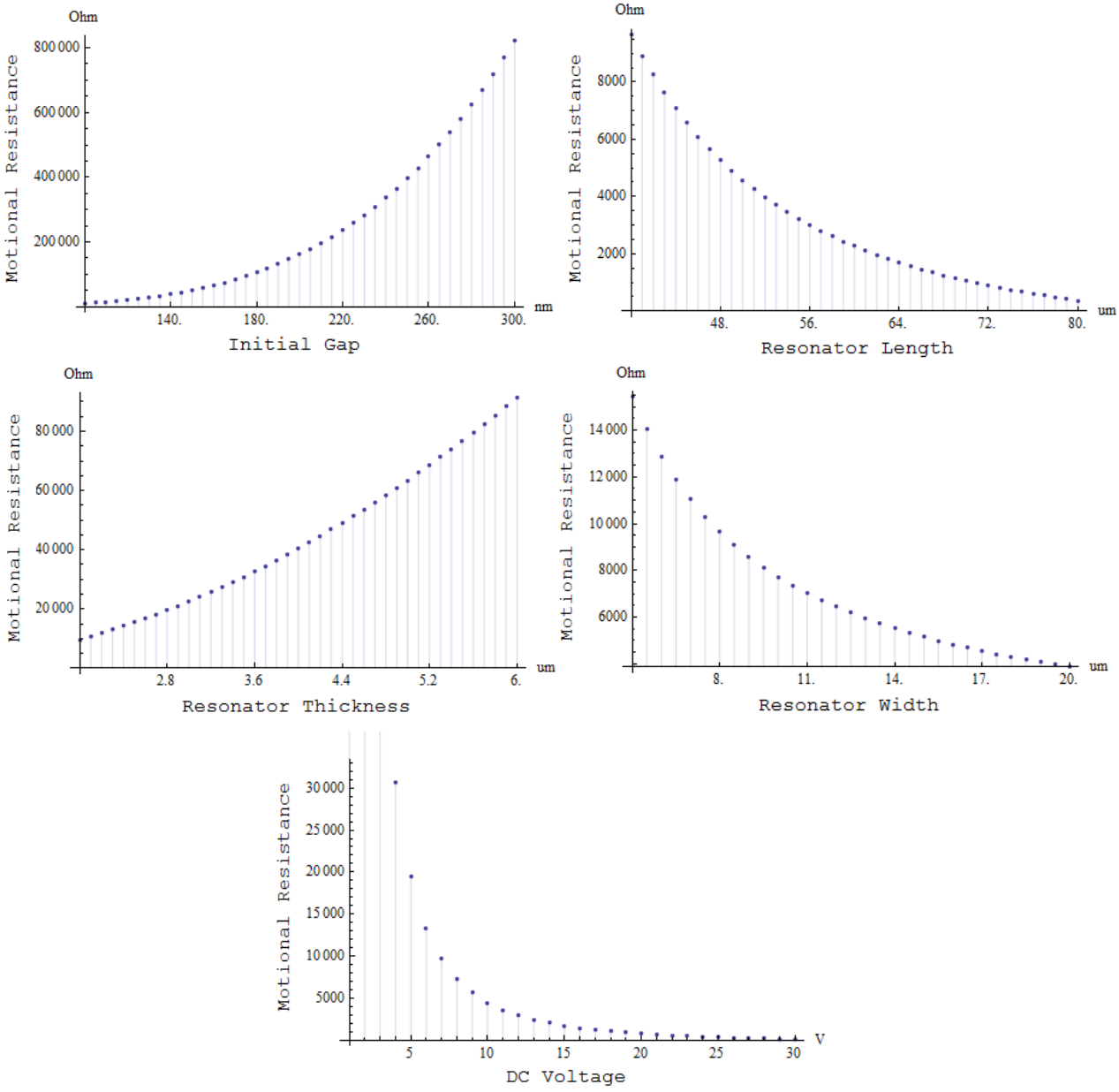

Figure 14 Motional resistance as a function of resonator initial gap, length, thickness, width, and DC bias

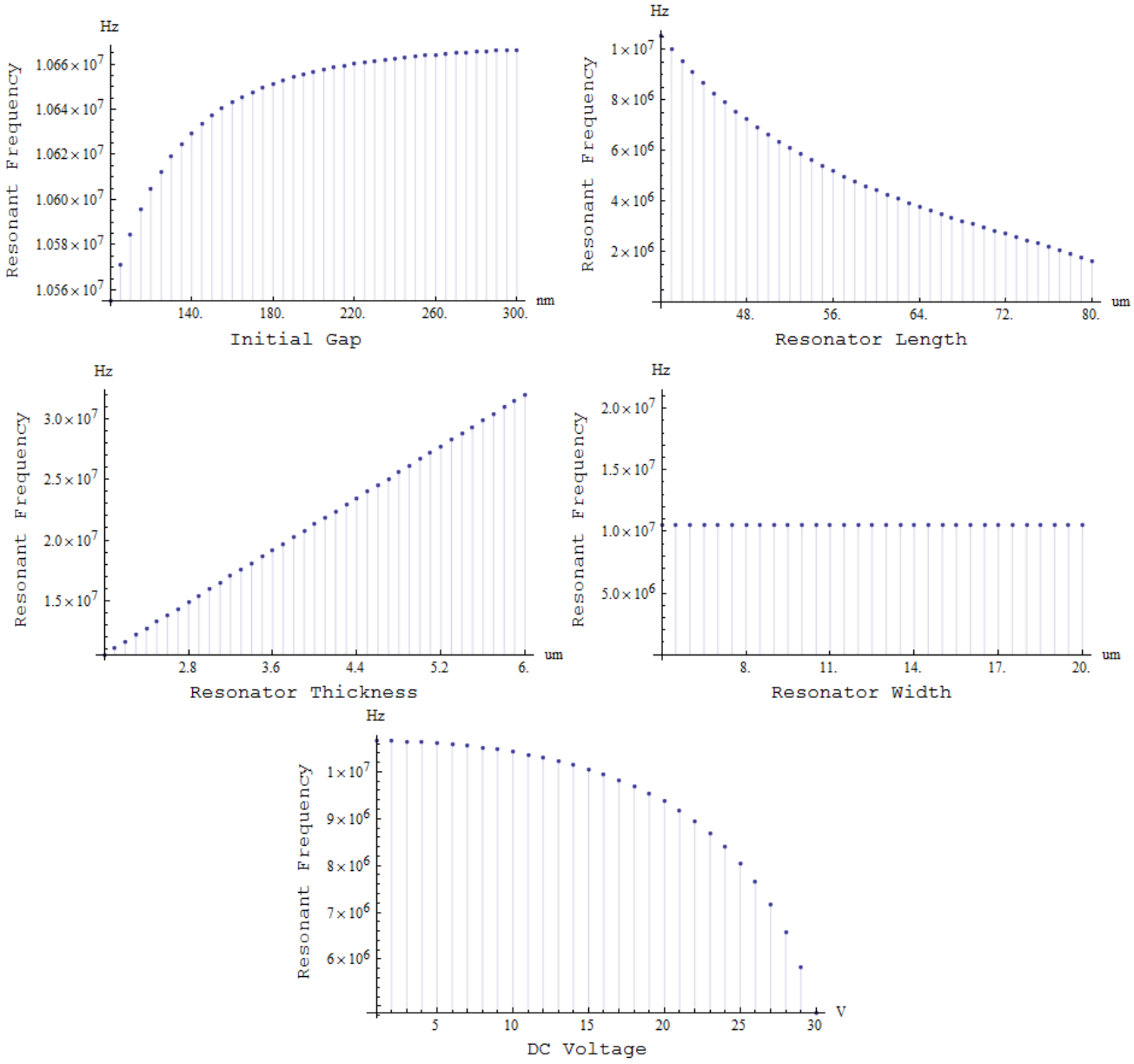

Figure 15 Resonant frequency as a function of resonator initial gap, length, thickness, width, and DC bias

However, the main figures of merit that would be interesting for RF filter design are S_{11} and S_{21} parameters. For the 1st CC beam resonator defined in Table 3-2, S parameter analysis was carried out

for changing values of Q (which would correspond to operation in different environments: air or vacuum) and values of DC bias (Figure 16 and Figure 17).

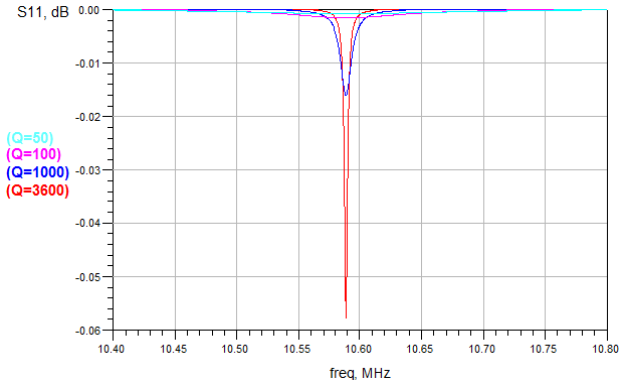

Figure 16 S11 parameter of the resonator for different Q factor values

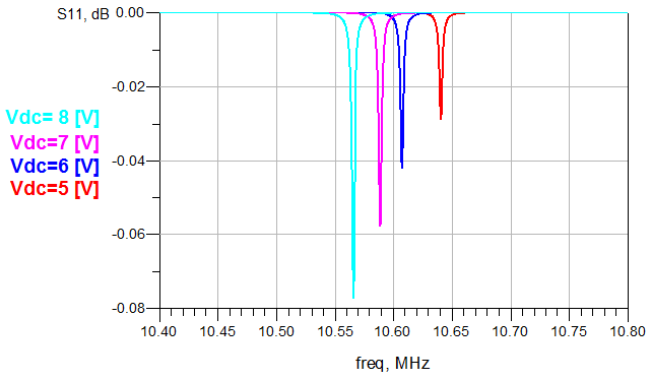

Figure 17 S11 parameter of the resonator for different Vdc values

As one may observe, S11 parameters of the resonator are significantly influenced by both the Q factor and the DC bias due to changes in electro-mechanical coupling efficiency.

Considering the above, one may formulate guidelines for designing moving mechanical structures (i.e., CC beams) of RSG-FET resonators. Based on the required specifications (e.g., resonance frequency, operating voltage, area) one needs to choose a length of the beam while keeping its width as broad as possible and its thickness as small as possible. These considerations would increase electro-mechanical coupling efficiency and thus lead to lower values of motional resistance.

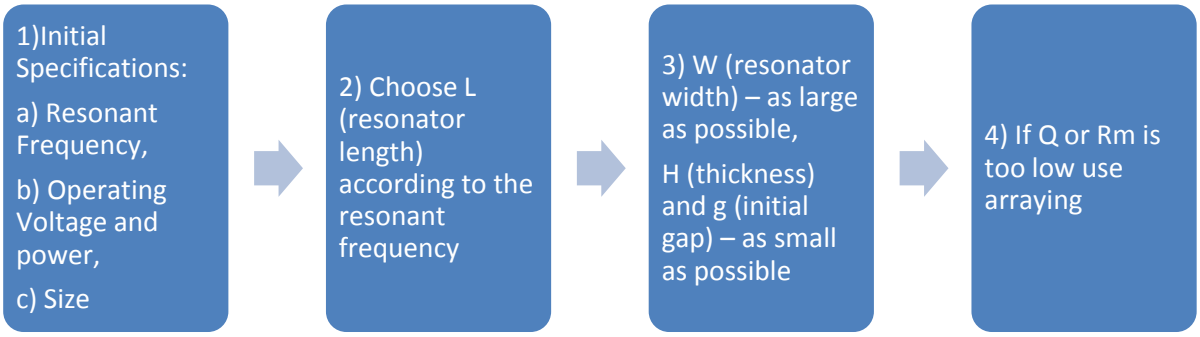

Figure 18 Guidelines for suspended gate design

If the desired values of quality factor or motional resistance are still not achieved, one may use an array of several resonators through mechanical coupling elements.

3.1.4 Mechanical Coupling Elements

Several improvements, such as reduction of motional impedance and Q factor enhancement, can be attained with proper mechanical coupling. Furthermore, and as has been outlined above, RSG-FET-based resonators have a relatively high motional resistance due to the nature of electrostatic actuation, which makes it complicated to interface the resonator with conventional 50 Ohm characterization equipment. As shown in the previous section, resonator coupling increases with higher electrode areas and therefore decreases motional resistance. At the same time, however, increased length causes lower resonant frequency. The resonator width should thus be increased as much as possible, keeping its value significantly smaller than the resonator length in order to preserve an approximation of a mechanical beam. One possible solution might be the high-velocity coupling of several identical resonators. In this way, the effective width and thus the coupling efficiency increases, preserving an approximation of a mechanical beam.

While the first intuitive approach of summation of the resonators output currents might be attractive in theory, in order to implement it in real life, the arrayed resonators must have exactly the same resonant frequency, which is hardly feasible due to fabrication tolerances. The approach thus leads to severe undesirable spurious modes.

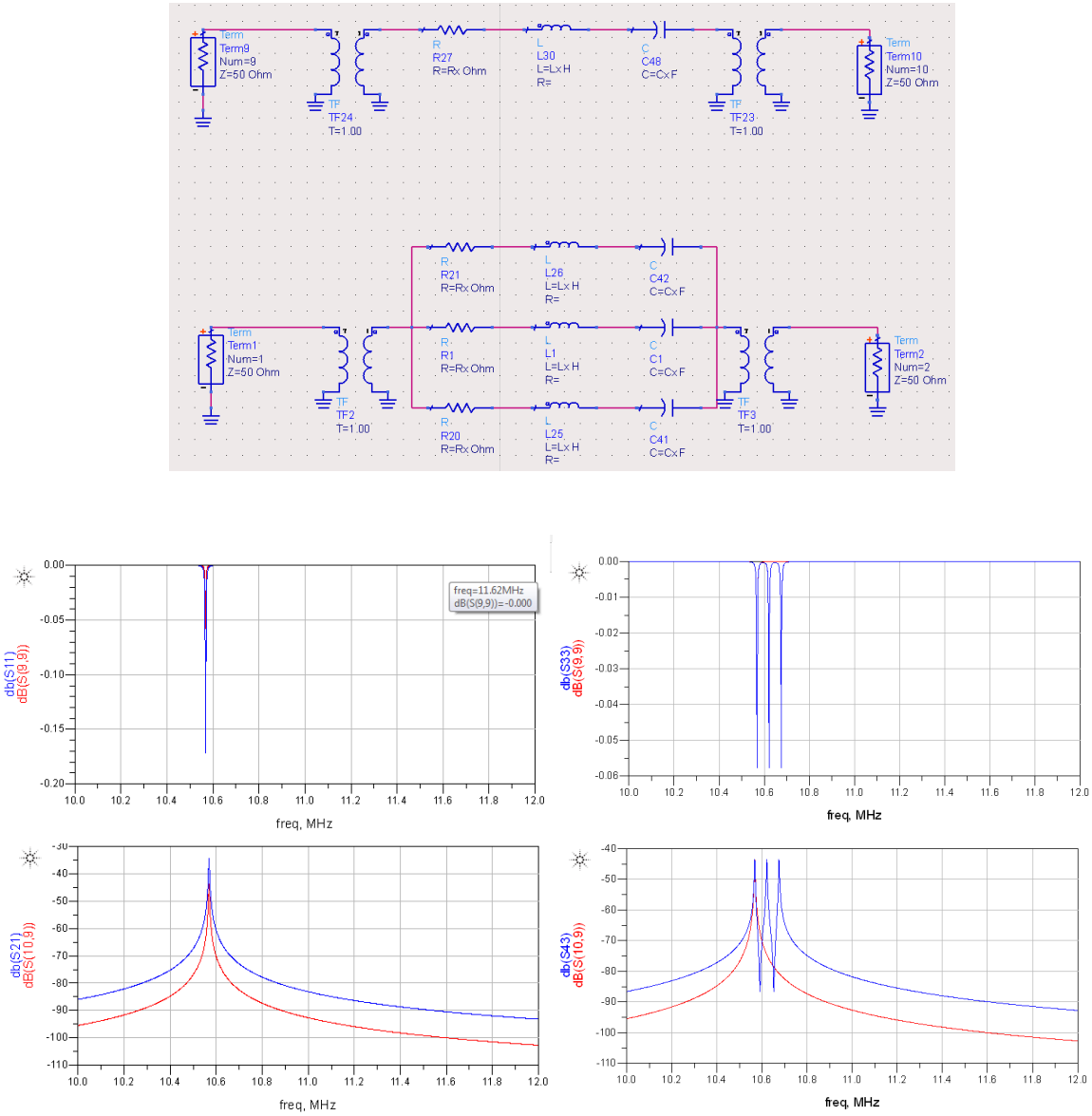

Figure 19 Impedance mismatch reduction via output current summation: a) equivalent circuits of a single resonator (top) and coupled resonators (bottom), b) S-parameters for a single resonator (red) and coupled resonators with the same resonance frequency (blue), c) S-parameters for a single resonator (red) and coupled resonators with different resonance frequency

Another approach to reduce the overall motional resistance is to array several identical resonators through short and stiff beams. This approach allows for the suppression of the spurious modes and moves them as far as possible from the band of interest. When the overall filter structure vibrates at a given modal frequency, all coupled resonators vibrate at this frequency. So, the main goal is to design the coupled array of resonators in such a way that one desired mode is emphasized and the others are suppressed. To achieve this goal, it is advantageous to separate the modes as far as possible [36].

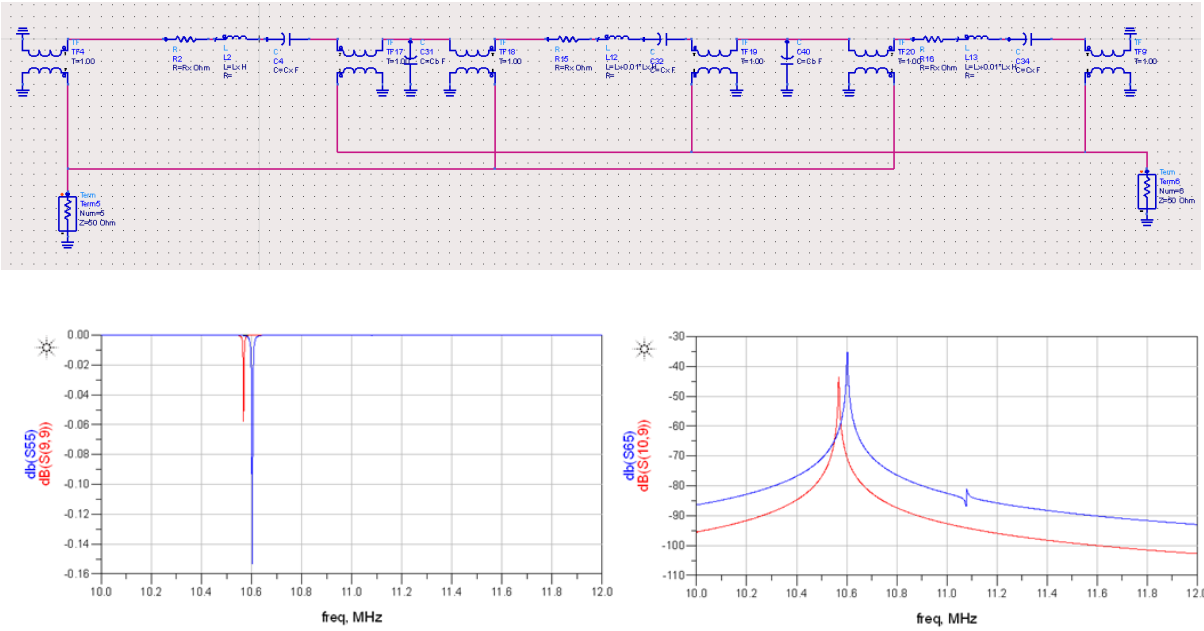

Figure 20 Impedance mismatch reduction via high velocity coupling: a) equivalent circuit of coupled resonators with slightly different resonance frequencies, b) S-parameters

As was shown earlier, a good Q factor of the resonator is essential. It can also be improved using $\lambda/4$ coupling of several resonators, thus improving the ability to store the energy of the overall arrayed system.

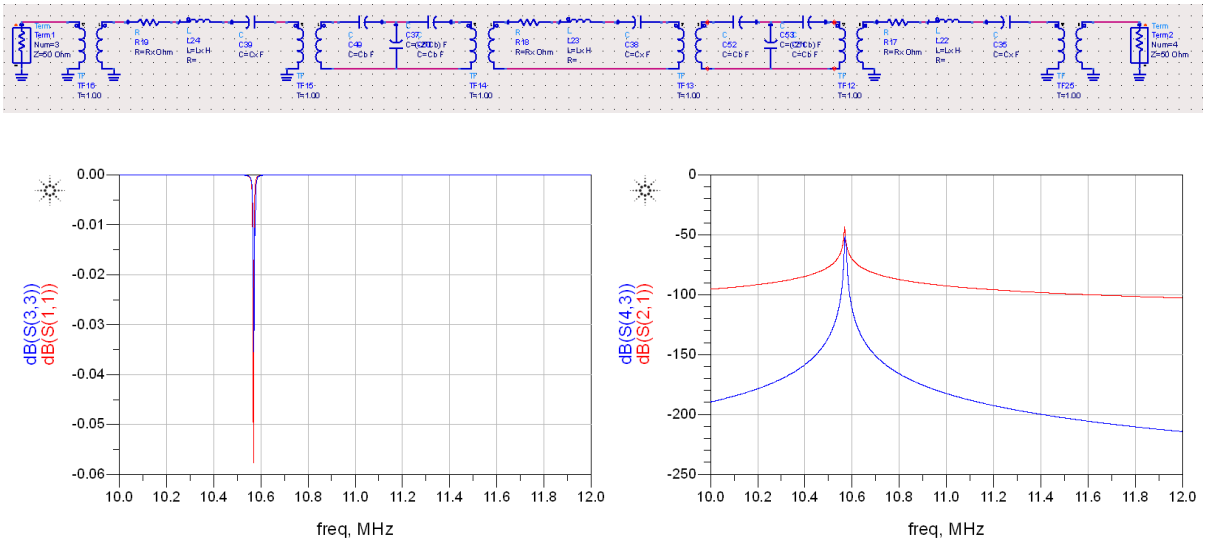

Figure 21 Q factor enhancement via mechanical coupling: a) equivalent circuit, b) S-parameters

Several high-velocity coupled CC beam-based resonator arrays have been designed to accentuate the first resonance mode and suppress the unwanted ones (Table 3-3).

Table 3-3. High-Velocity Coupled CC-Based Resonator Arrays

№	Structural materials	resonator l [um]	resonator w [um]	Thickness h [um]	coupling beam width [um]	coupling beam length [um]	calculated lambda/8	Number of resonators coupled	f0 (aimed) [Hz]	f0 (FEM) [Hz]
1	$SiO_2 + M_1 + SiO_2 + M_4$	70	6	6.515	4	4	97.8519	4	7.21E+06	6.98E+06
2	$SiO_2 + M_1 + SiO_2 + M_4$	50	6	6.515	4	4	52.0777	4	1.35E+07	1.30E+07
3	$SiO_2 + M_1 + SiO_2 + M_3$	70	6	4.59	4	4	136.299	4	5.17E+06	5.02E+06
4	$SiO_2 + M_1 + SiO_2 + M_3$	50	6	4.59	4	4	71.093	4	9.92E+06	9.53E+06

Figure 22 shows the fundamental mode of high-velocity coupled resonator arrays with two and four CC beams. We can see that high-velocity coupled arrays lead to increased coupling efficiency and thus to smaller motional resistance.

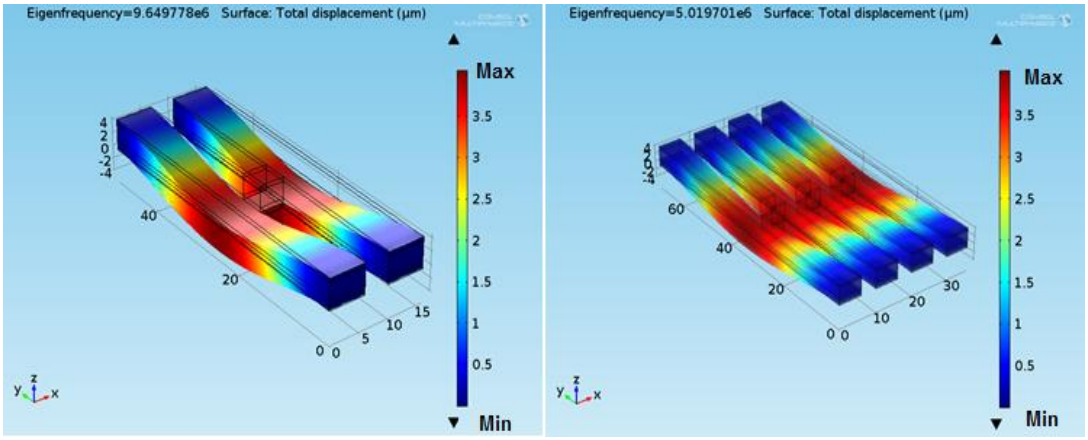

Figure 22 Fundamental mode of high-velocity coupled resonator array: a) two resonators, b) four resonators

Bandpass filter response can also be implemented using several identical inter-coupled resonators. Generally, a system of two identical coupled resonators has two mechanical-resonance modes with closely-spaced frequencies (in-phase and out-of-phase) that form the filter passband, which is given by:

$$BW = f_0 \frac{k_{c1} + k_{c2}}{k_r}, \tag{3-10}$$

where f_0 is the resonator resonance frequency, k_r is resonator effective stiffness, and k_{c1} and k_{c2} are in-phase and out-of-phase coupling beam effective stiffness, respectively.

As shown in the previous section, the resonator dynamic mass and its stiffness are strong functions of velocity, given by the expressions:

$$m_r = \frac{KE_{tot}}{\frac{1}{2}\, v_c^2}, k_r = \omega_0^2\, m_r, \tag{3-11}$$

where KE_{tot} is the total kinetic energy and v_c is the maximum resonance velocity at location c on the resonator. As a result, the resonator lowest stiffness is observed at the location of the maximum velocity. Short coupling beams ensure higher coupling stiffness. All this separates the modes of the resonator as far as possible, accentuating the first mode and suppressing the others.

The FEM analysis of bandpass mechanical filter structure with reduced motional resistance via coupling is shown below.

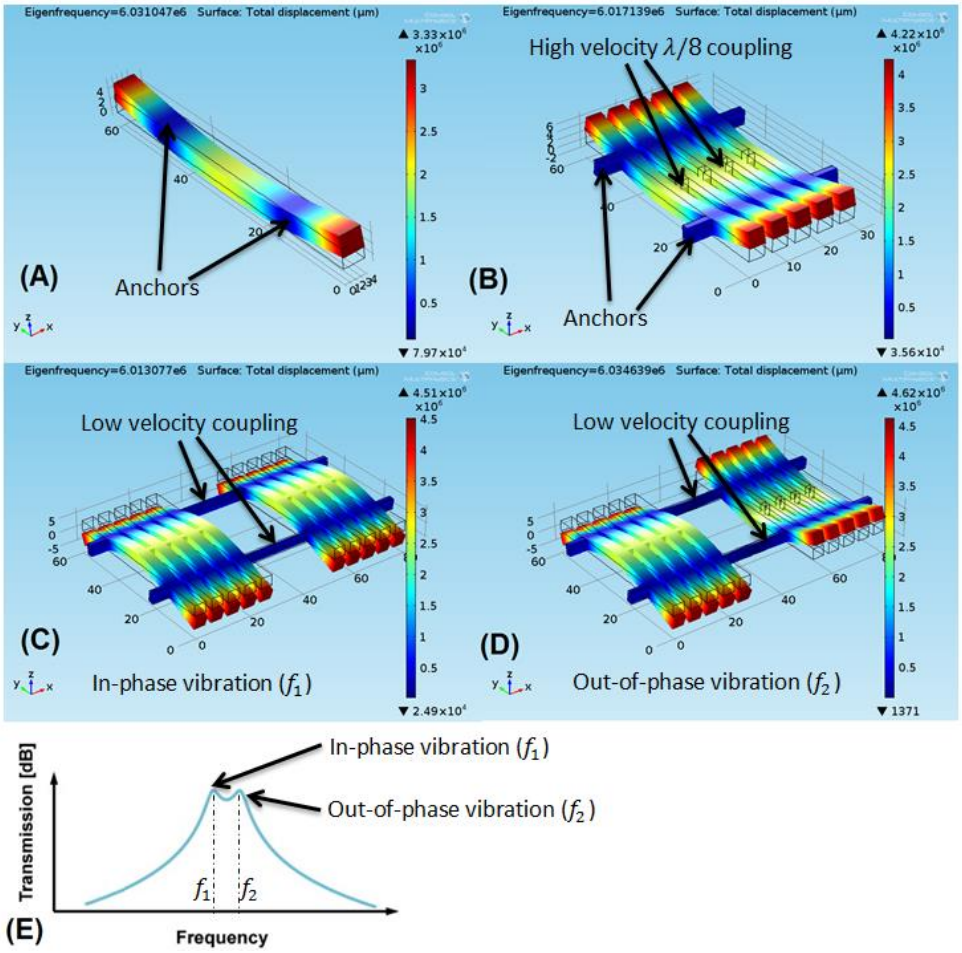

Figure 23 Mechanical bandpass structure: a) single beam resonator, b) high velocity coupled resonator, c) in-phase vibration of the structure, d) out-of-phase vibration of the structure

3.2 MOSFET Readout

In order to utilize the CMOS MOSFET as readouts, the TSMC-fabricated MOSFETs were characterized (i.e., electron mobility, threshold voltage, etc). In simulations, it was done using the provided CMOSP35 kit.

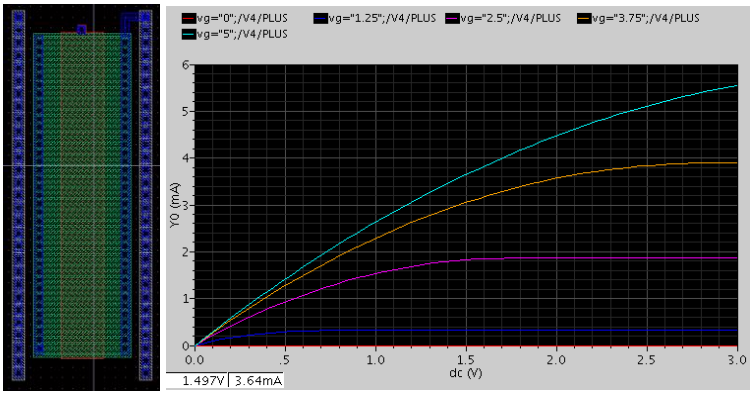

Figure 24. CMOSP35 MOSFET: layout and Id-Vd curves (W=30 um, L=4 um)

However, fabricated MOSFETs showed parameter degradation, which occurred during the post-CMOS fabrication process.

It is also important to keep in mind that the RSG-FET threshold voltage increases significantly due to the air gap created to release the moving mechanical structures, which has a lower dielectric constant and significantly higher thickness. Thus, the RSG-FET-based resonator should be biased properly in order for the conductive channel to be opened. As shown below, if the gate dielectric is replaced by an air gap with a thickness of 200 nm, the threshold voltage of the MOSFET increases from 0.8 V up to 38 V.

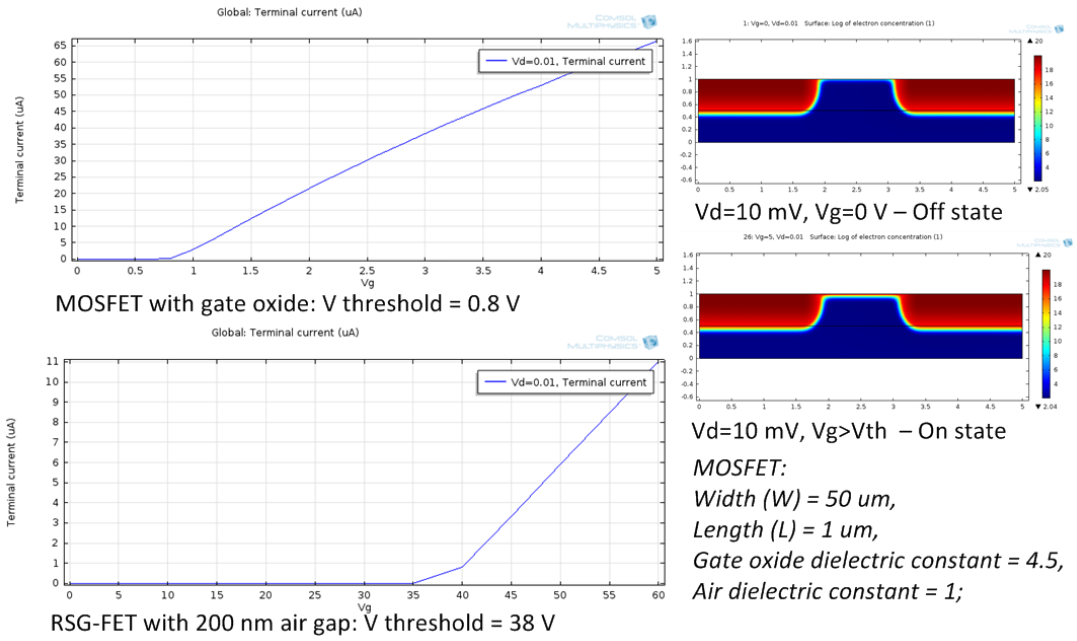

Figure 25 FEM analysis of MOSFET: a) Id-Vg curves for conventional MOSFET, b) Id-Vg curves for RSG-FET, c) On and Off state of conductive channel

The conclusion here is that one needs to keep the air gap as small as possible to achieve the desired efficiency of MOSFET readouts. Modern FEM tools are capable of simulating multiphysics problems (i.e., solid mechanics, semiconductors, electrodynamics coupled together). This allows us to estimate the approximate value of the output drain current when the vibrating gate is in resonance.

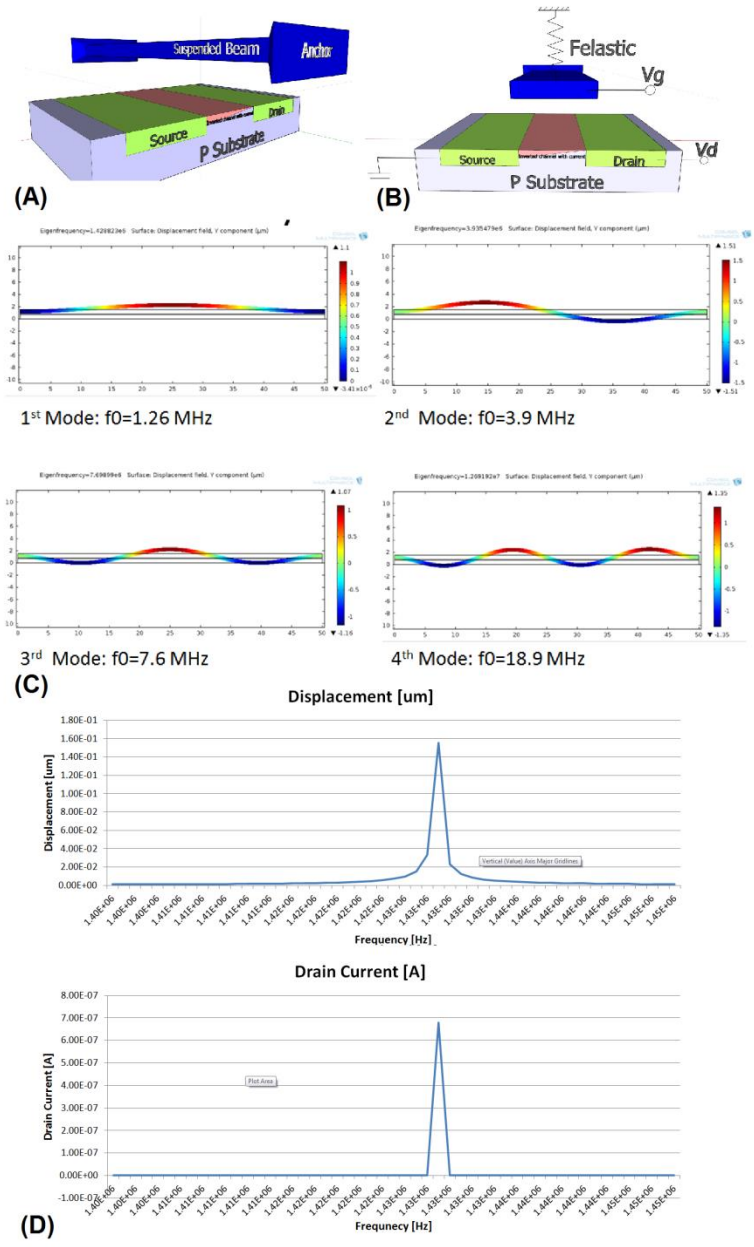

Figure 26 RGFET-based resonator: a) 3D structure, b) cross-section and biasing, c) mode shapes of the suspended gate, d) displacement and MOSFET current of a single RGFET resonator as a function of actuation frequency ($V_{drain} = 10\ mV, V_{gate}^{DC} = 10\ V, V_{gate}^{AC} = 0.1\ V$)

An equivalent circuit model of RSF-FET was built using an equivalent model of an electrostatically driven suspended gate and the transistor model (TSMC CMOSP35 kit). The RSG-FET was used in a common source configuration to estimate the output voltage (AC) at resonance.

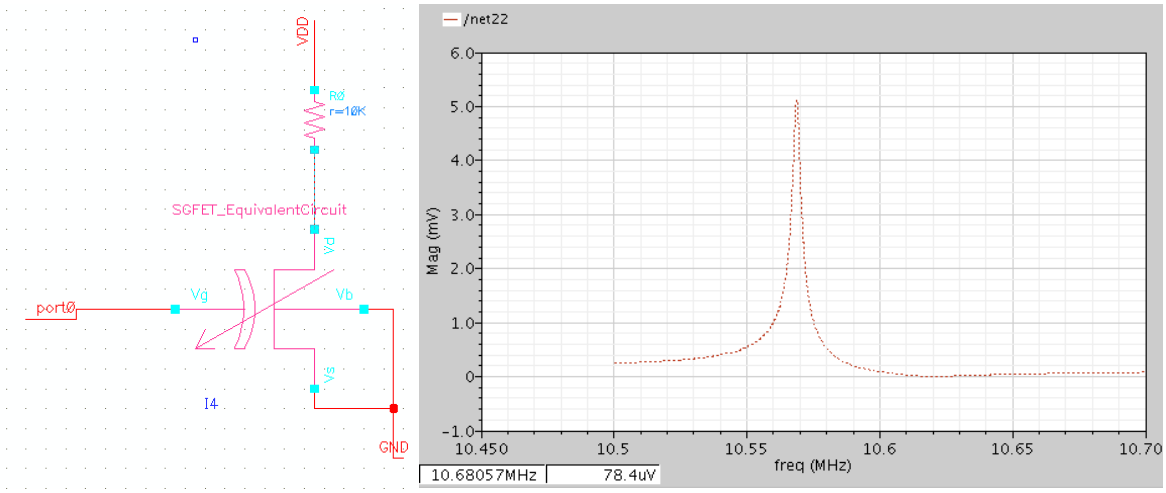

Figure 27 RSG-FET-equivalent circuit (left) and output voltage (right)

All of the models described above can give a rough estimation of the expected output signal values from an RSG-FET-based CMOS-MEMS resonator. The information could be successfully used in building more complicated block-like filters, oscillators, etc.

3.3 Chapter Summary

This chapter presented a lumped, distributed and FEM analysis of a mechanical suspended gate. Based on this analysis, design guidelines were formulated. Different coupling techniques for impedance mismatch reduction and Q factor enhancement were described and analyzed via equivalent models. The last section contains multiphysics FEM and lumped analysis of RSG-FET.

Chapter 4

4.1 Post-CMOS Fabrication Process

As outlined in Chapter 2, in order to attain higher values of resonator Q, it is necessary to reduce its motional resistance, which means decreasing the gap size. With the use of a CMOS-MEMS post-process of foundry-fabricated chips and some mechanical design techniques, high Q resonators can potentially be achieved.

Cross-sections of material stacks for TSMC CMOSP35 and CMOSP18 are depicted in Figure 28. With additional post-processing steps (e.g., thin film etching and bulk Si etching using a top metal layer as a mask), mature CMOS processes can be used as a fabrication platform for MEMS.

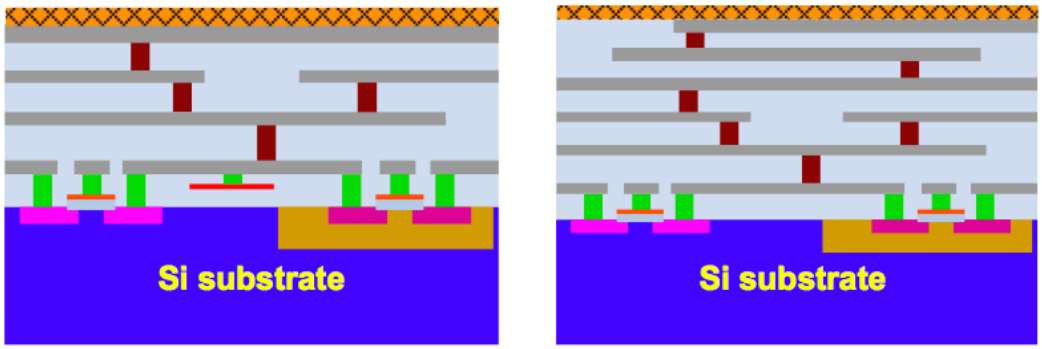

Figure 28 Material stacks for 0.35 μm 2P4M CMOS process and 0.18 μm 1P6M CMOS process

Electrode-to-resonator gap spacing can be implemented by using one of the CMOS layers as a sacrificial layer. In this way, the resonator motional resistance is limited by the minimum feature size of the current CMOS process. One of the metal or polysilicon layers can be used as a sacrificial layer to achieve the desired gap size, depending on the application. For example, to design a high Q

resonator using the CMOSP35 process, one can choose the polysilicon layer, as it is the thinnest. The subsections below outline several possible release processes.

4.1.1 CMOS-MEMS RSG-FET with Metal Sacrificial Layer

Using M1 as a sacrificial layer provides a gap of at least 0.6 μm. The release post-process consists of RIE silicon dioxide etch with CHF3 and wet aluminum PAN etch (Figure 28).

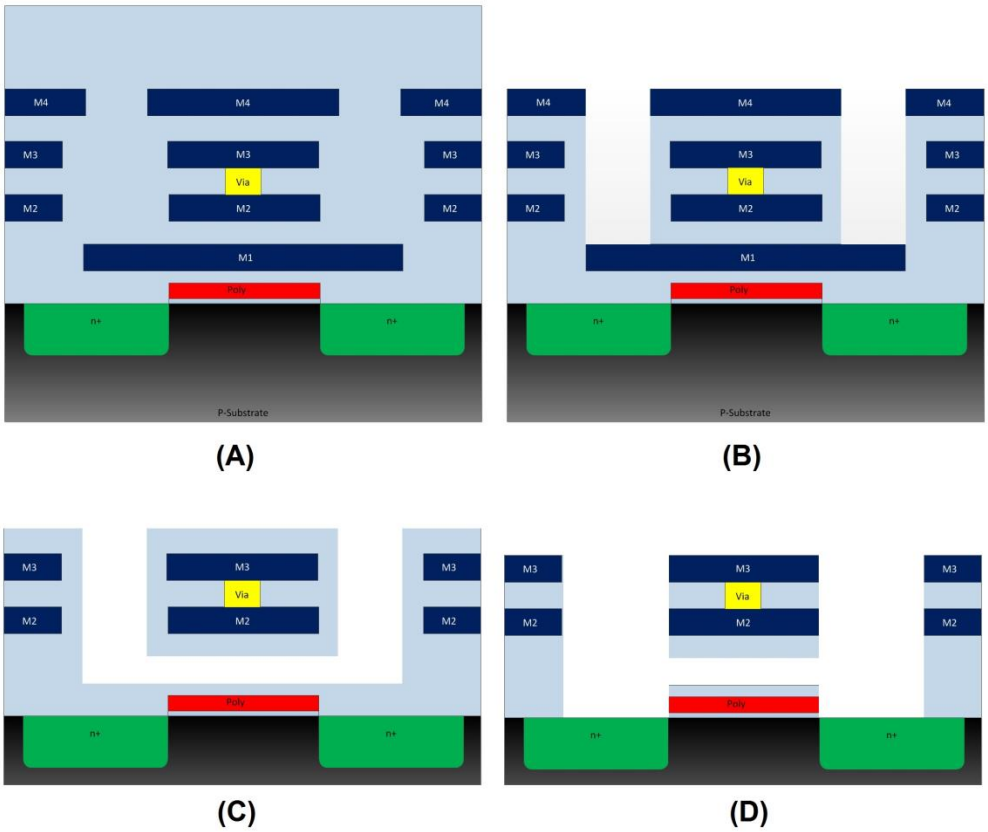

Figure 29 Post-process steps: a) foundry-fabricated CMOS chip, b) dry silicon dioxide reactive ion etching, c) wet aluminum PAN etch, d) dry silicon dioxide reactive ion etching

To prevent stiction of the released gate on the substrate, CO2 drying is used after the wet etch step.

4.1.2 CMOS-MEMS RSG-FET with Polysilicon Sacrificial Layer

Using Poly2 as a sacrificial layer provides a gap of at least 0.2 μm. The release post process consists of RIE silicon dioxide etching with CHF3 and RIE polisilicon SF6 etching.

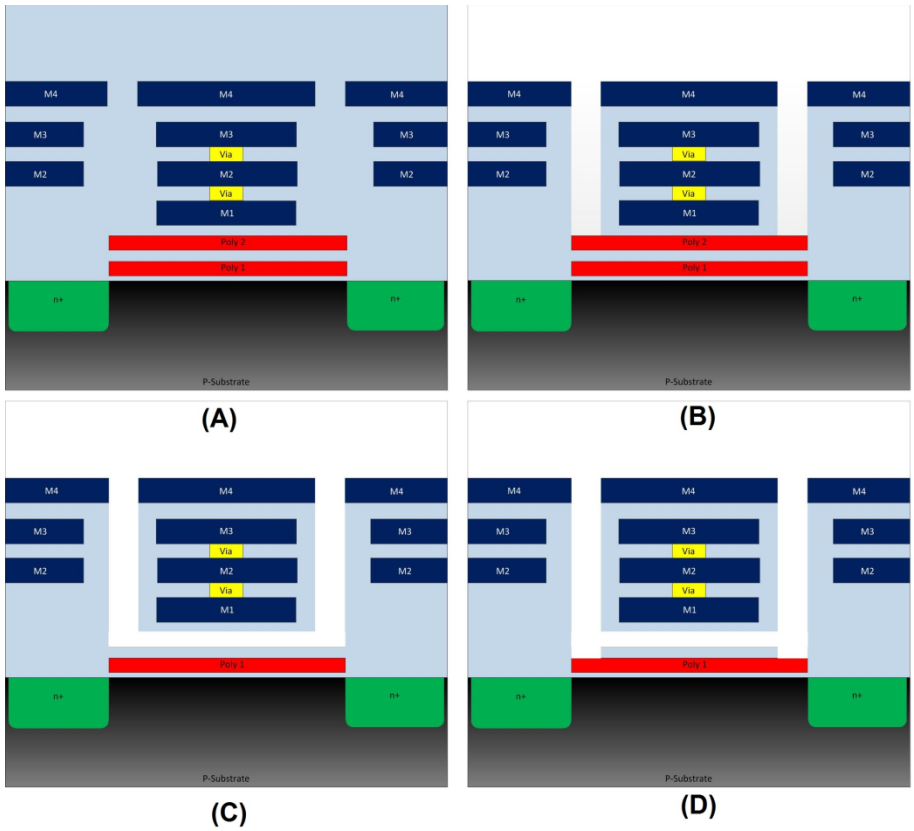

Figure 30 Post-process steps: a) foundry-fabricated CMOS chip, b) dry silicon dioxide reactive ion etching, c) wet polysilicon TMAH etching, and d) dry silicon dioxide reactive ion etching

Another way to reduce the gap would be using design techniques such as additional actuators to bring the suspended gate closer to the substrate or pull-in stoppers to land on.

As can be seen, the post-process of CMOS-MEMS is vital for high Q nano-mechanical resonators. However, it may damage the silicon substrate surface, which would lead to a decay of the MOSFET

performance. Hence, the best post-process must be chosen to keep the silicon surface as protected as possible.

4.1.3 SEM Characterization of RSG-FET-Based CMOS-MEMS Resonators

In order to achieve a higher yield through the fabrication cycle, one needs to keep the number of post-processing steps as low as possible. It is also better to avoid using wet etch steps due to their relatively low reproducibility and limited controllability. Various types of RSG-FET-based CMOS-MEMS resonators were fabricated in the CIRFE in-house clean room facility.

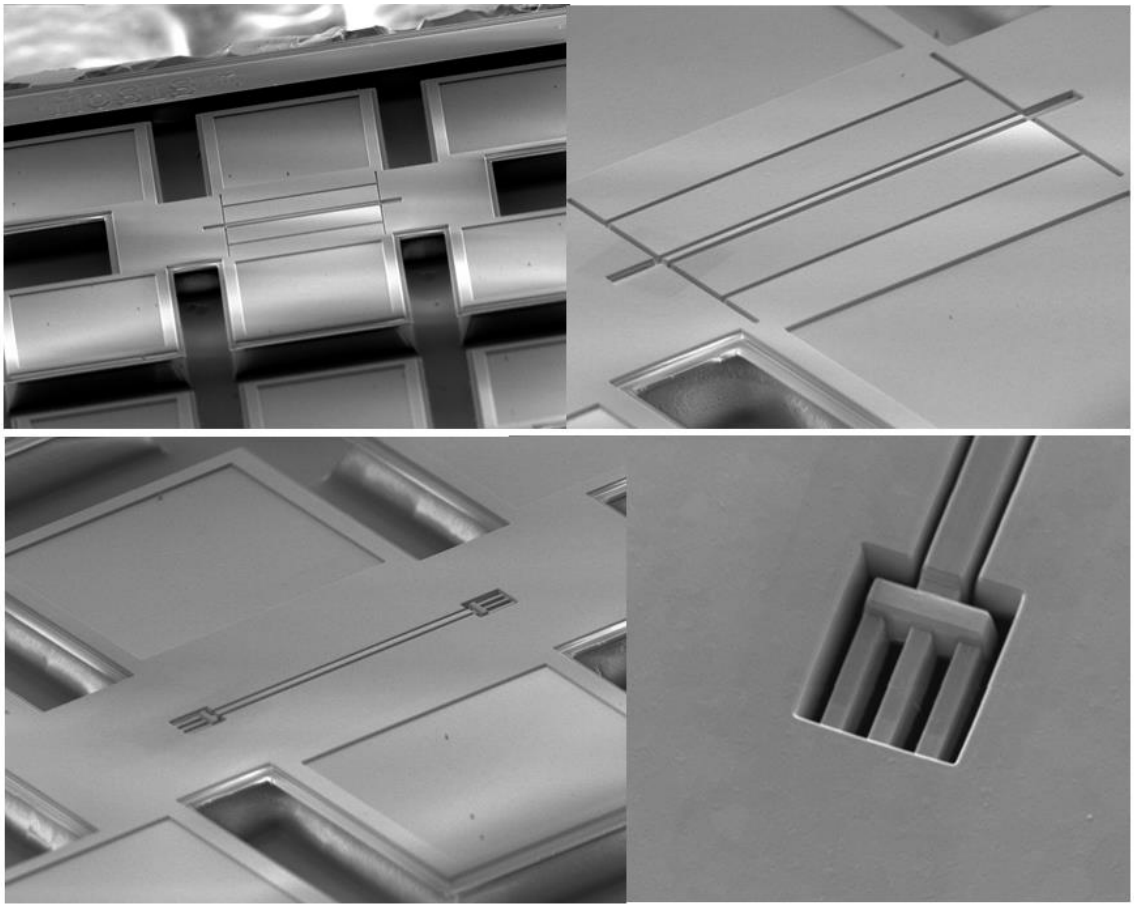

Figure 31. SEM pictures of released RGFET-based MEMS devices

Examples of successful POST-CMOS fabrication are shown above. Despite the success, there is still room for improvement.

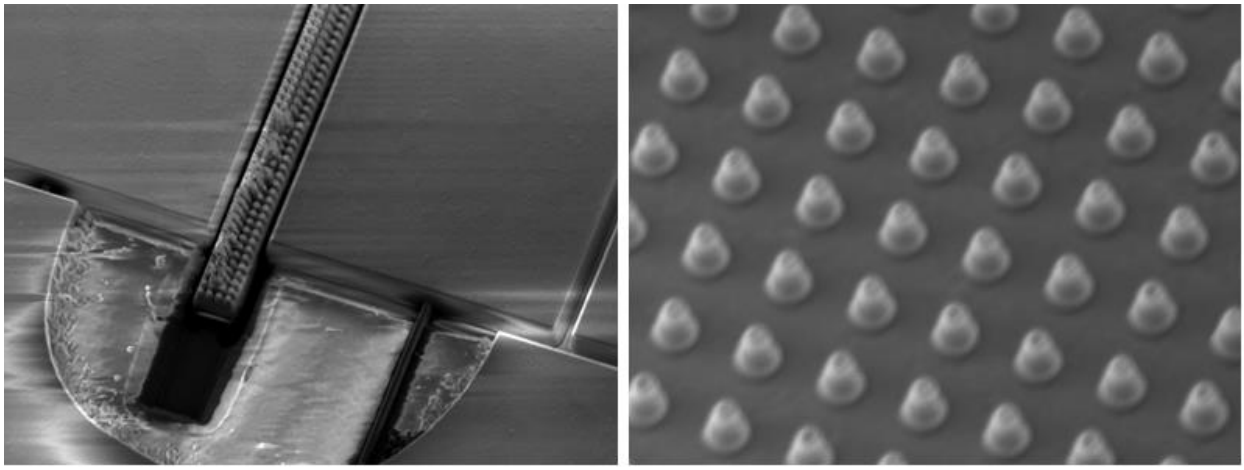

Figure 32 Post-CMOS fabrication process failures

Some process failures are shown in Figure 32, which are attributed to CMOS chip internal stress, over-etching and over-heating during the wet-etch step.

4.2 Dynamic Characterization Using Laser Doppler Vibrometer

The dynamic response of RGFET MEMS was characterized by a laser vibrometer (Figure 33). The experimental setup and biasing are shown below.

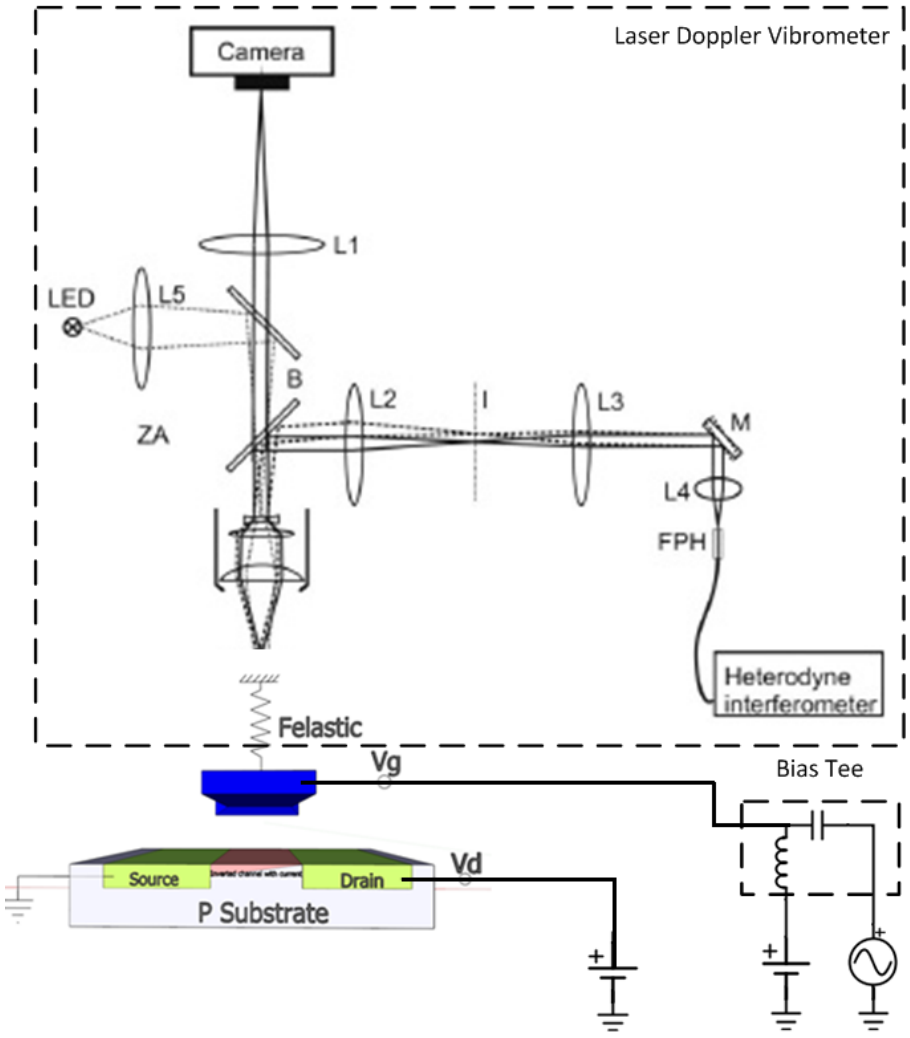

Figure 33 Laser Doppler vibrometer experimental setup

The measurements show that some of the CC beams are partially released with an effective length of two-thirds of the designed value (Figure 34b), which necessitates the improvement of the fabrication process. The frequency response of the vibrating CC beam is given in Figure 34c. The fundamental resonance peak is clearly observed and its frequency (480 kHz) matches the theoretical and FEM

simulated value, when accounting for a smaller effective length and the electrical softening phenomenon.

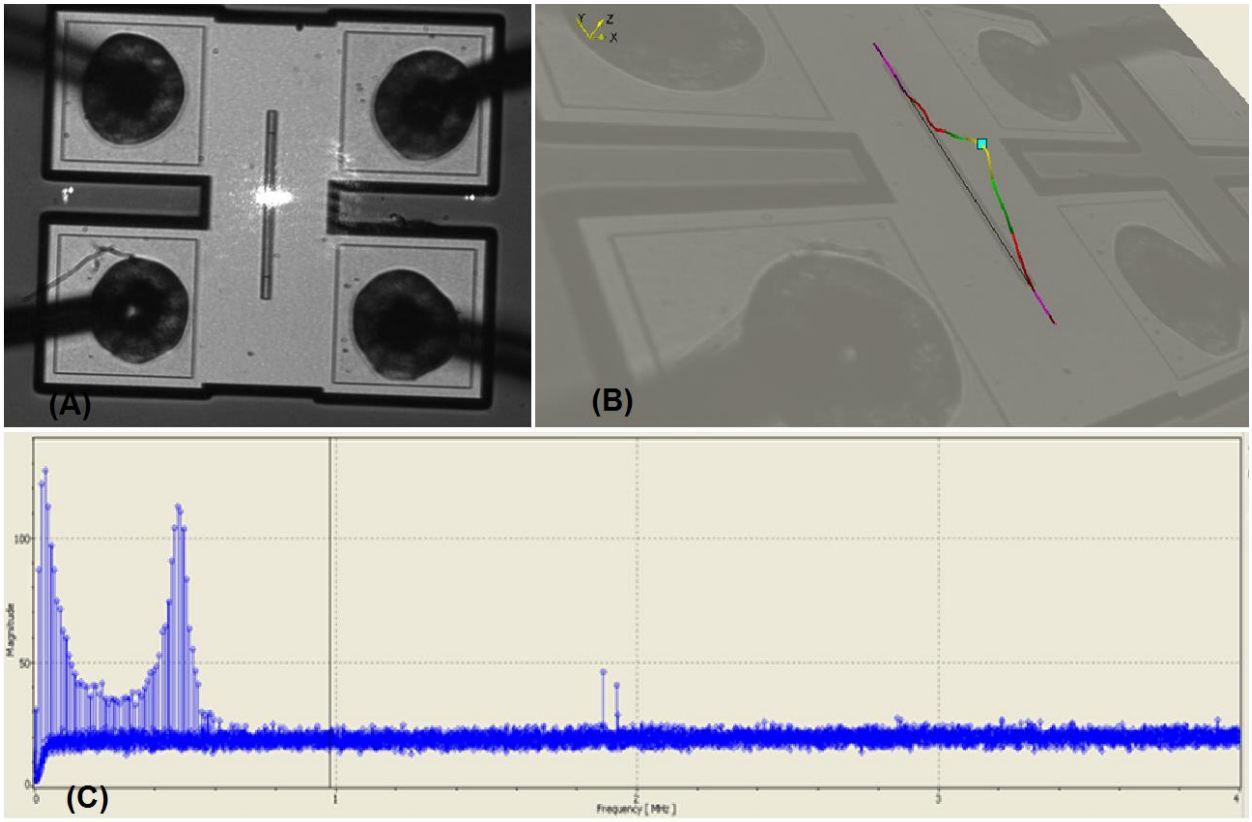

Figure 34 Laser vibrometer measurements: a) CC beam and laser under microscope, b) CC beam deflection profile, c) frequency response of the vibrating CC beam

As expected, stiffer MEMS structures show higher resonance frequency. The frequency response of the vibrating beam shows such important parameters as resonance frequency, Q factor, and maximum dynamic beam deflection.

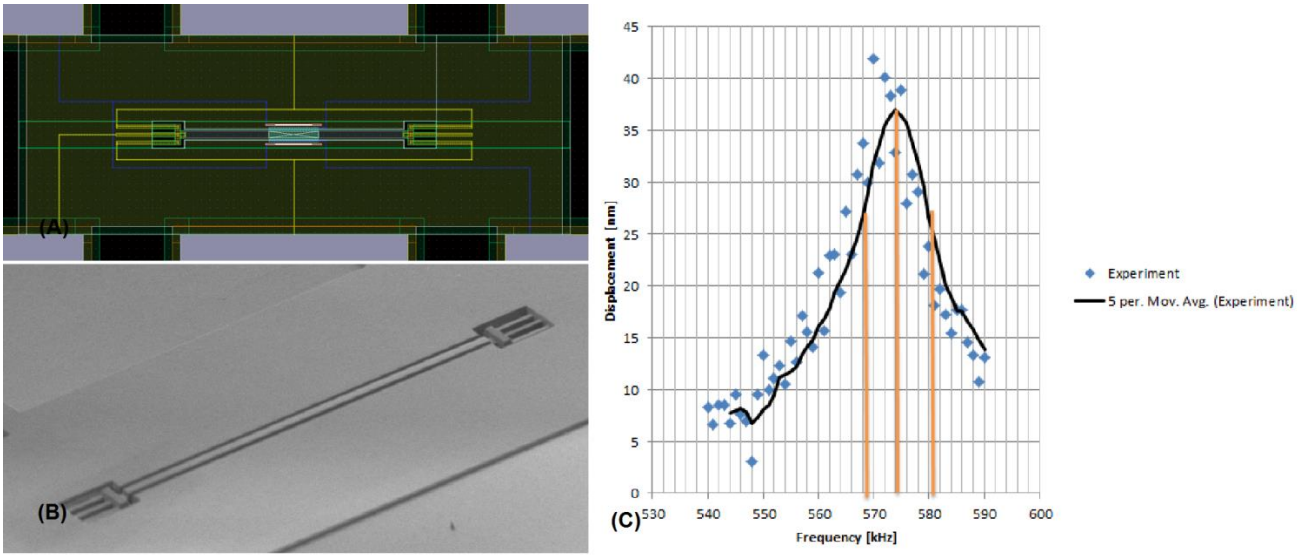

Figure 35 RGFET-based MEMS: a) layout, b) SEM picture, c) frequency response

Based on this information, one may extract the parameters relevant to electromechanical transduction and build an equivalent circuit model, which is vital for integration with CMOS analog electronics.

Table 4-1. Q-Factor Calculation Based on Frequency Response

	Displacement[nm]	**Frequency [kHz]**
Max	37	574
3dB1	25.9	568
3db2	25.9	580
Calculated Q factor (air)	**48**	

For the system depicted, a Q factor of 48 in air was calculated based on the laser vibrometer measurements. Performing the experiments in a vacuum will significantly reduce air damping, which will improve the overall Q factor of the system and decrease the motional impedance.

4.2.1 Resonance Frequency Tuning with DC Bias

As an electrostatically actuated transducer, RGFET inherits the beam spring constant softening phenomenon with applied DC voltage, thus providing an opportunity to tune its resonance frequency.

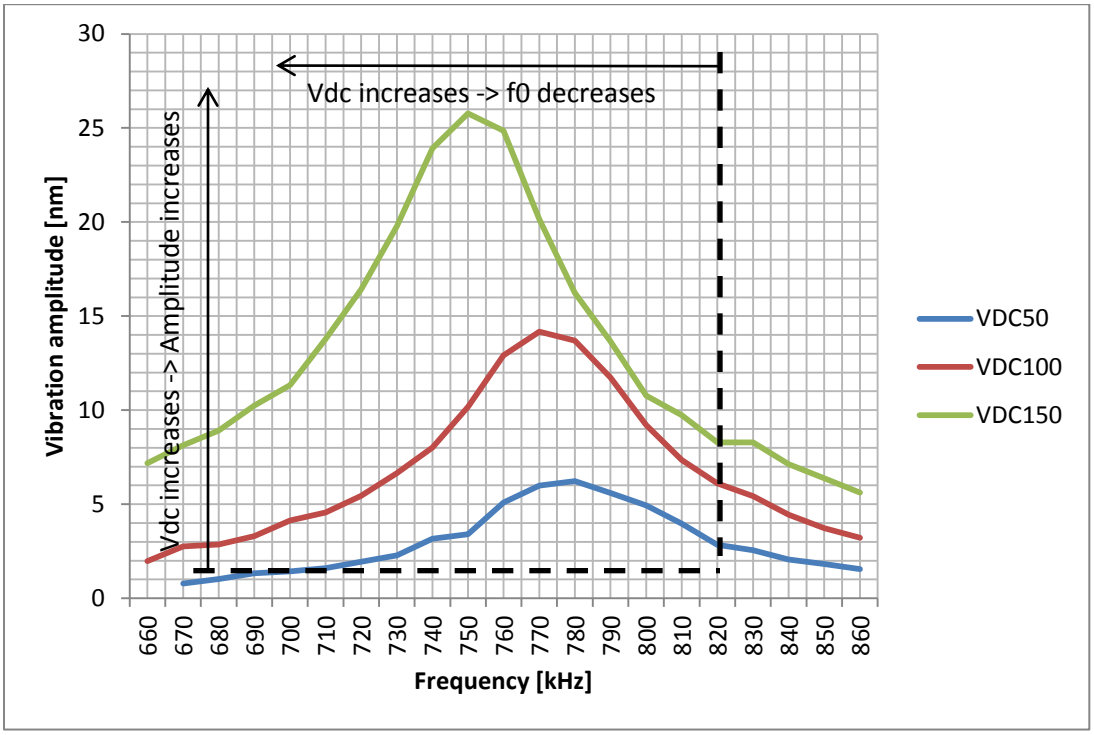

One may notice that the resonator resonance frequency decreases as the bias voltage increases, due to the decreased value of the effective stiffness of the beam (i.e., electrostatic softening). On the other hand, the vibration amplitude of the beam increases as the bias increases. This occurs due to the

increasing electro-mechanical coupling efficiency of electrostatic transduction and potentially leads to an increase of the output signal.

4.2.2 Resonance Frequency Tuning with Electrothermal Joule Heating

Even though RSG-FET comes with a ready-to-use intrinsic mechanism of tuning with DC bias, it has several disadvantages, such as maximum amplitude variation and the ability to reach pull-in instability, which may cause suspended gate collapse and chip destruction. Hence, combined electrostatic/electrothermal systems are of the most interest here. The system is built such that electrostatic transduction drives the device into a resonance, while the heaters, which are made of poly1, are embedded directly into the resonator and used to tune the resonance frequency.

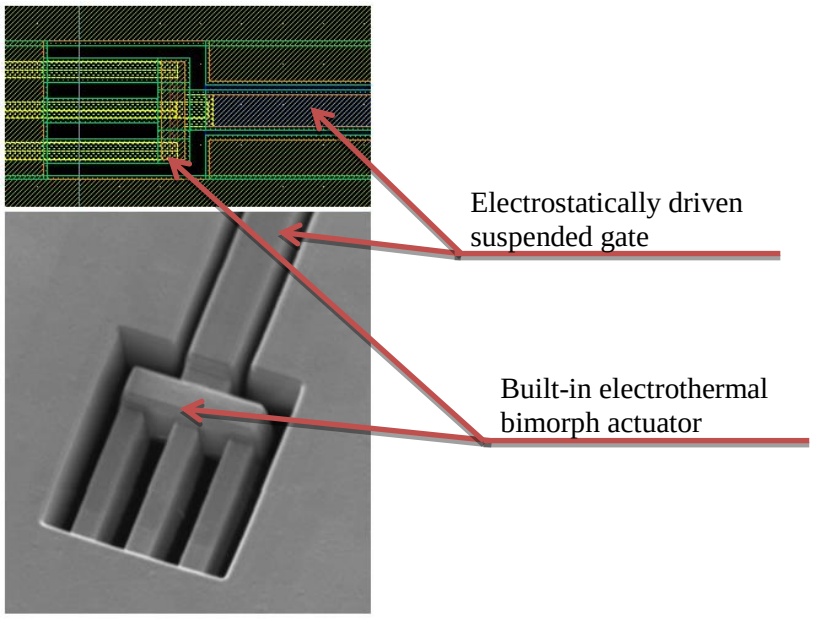

Figure 36 RSG-FET with integrated electrothermal bimorph actuator

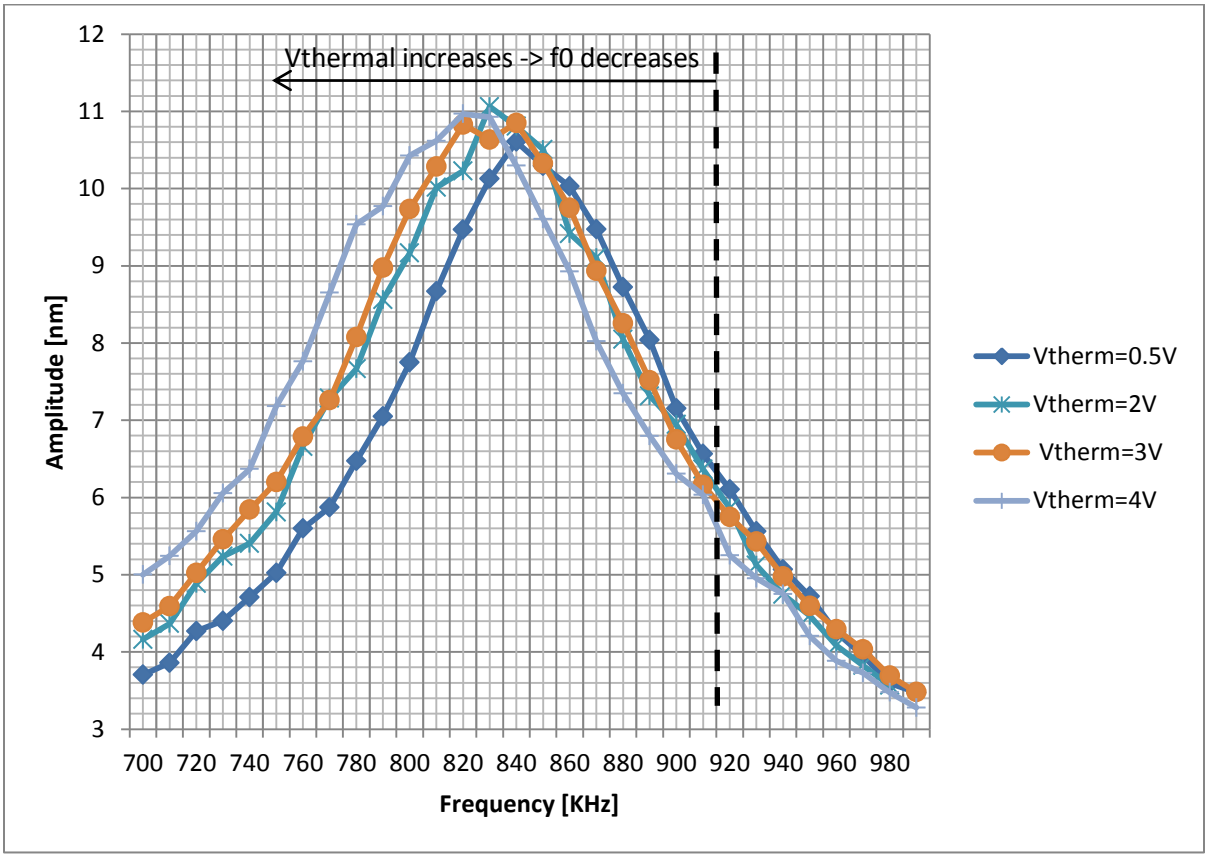

The electrothermal approach is an additional way to tune the resonator resonance frequency. It has the advantage of avoiding pull-in instabilities at a cost of increased power consumption and more complicated designs.

4.3 Electrical Characterization with Lock-In Amplifier

To characterize the electrical output signal, the RSG-FET is used in a common source amplifier configuration. The HF2LI Lock-In Amplifier (Zurich Instruments) was used to supply an input AC signal and read the output signal at different frequencies. The obtained magnitude of the output signal

as a function of frequency provides necessary information about where the resonance occurs. RSG-FET-based resonators with 70 um long beams were used in this experiment.

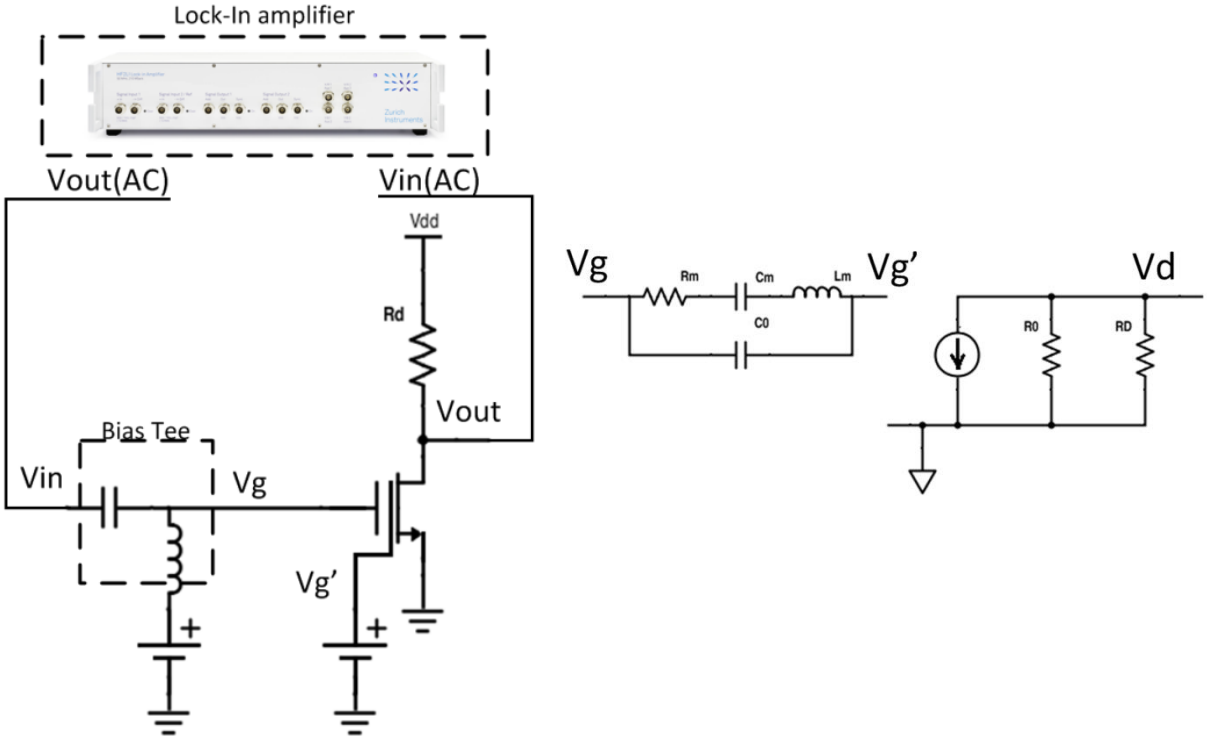

Figure 37 Experimental setup (left) and RSG-FET small signal model (right)

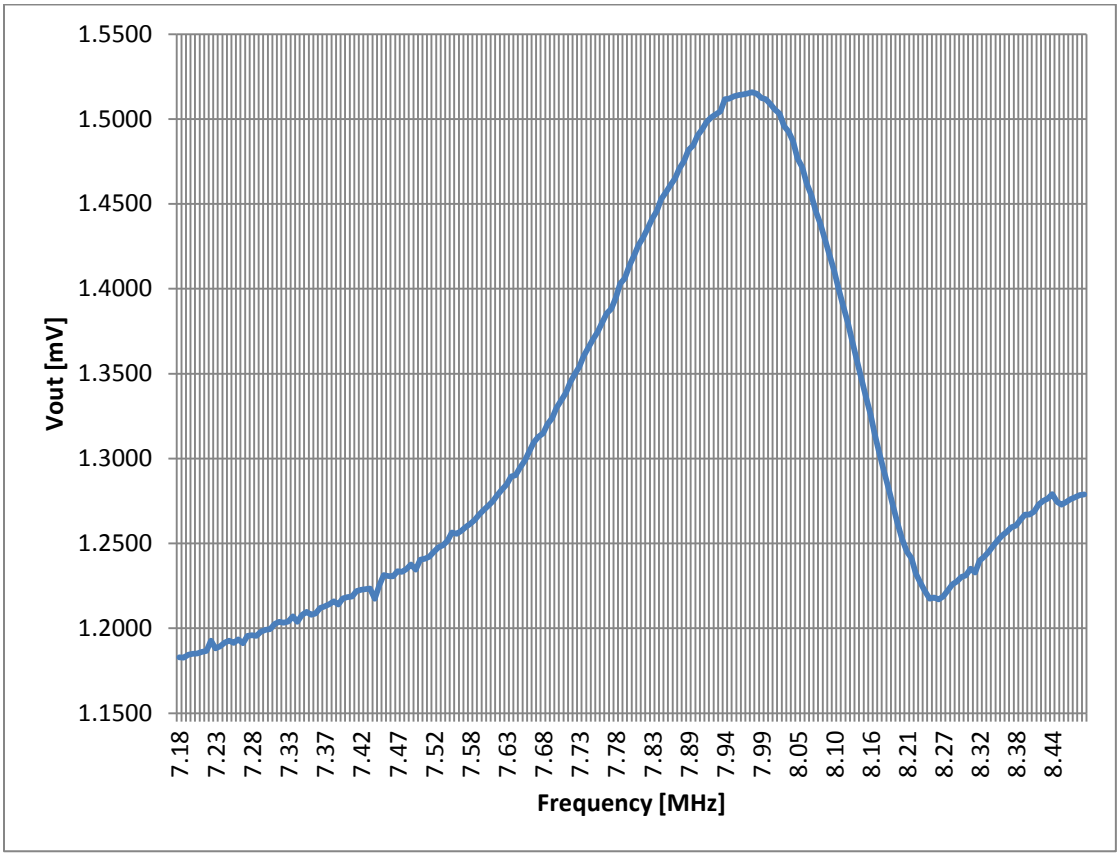

Figure 38 Output signal as a function of frequency

4.4 Chapter Summary

This chapter presented a description of post-CMOS fabrication steps and highlighted their advantages and disadvantages. The results show the successful release of the moving suspended gate without causing significant damage to the silicon surface. The process does, however, cause some degradation of MOSFET properties and has relatively low reproducibility and relatively high deviation of the resonators resonance frequency, Q factor, etc.

The second section of the chapter contained a description of characterization with a laser Doppler vibrometer and a lock-in amplifer. The results enabled the calculation of the actual resonance frequency of the devices and their Q factors. The resonator tenability, through DC bias and electrothermal actuation, was also experimentally investigated and verified in this chapter.

Chapter 5

5.1 Conclusions

The thesis presented the design and fabrication of a CMOS-MEMS Resonant Suspended Gate FET-based resonator. The first half of the work described the lumped, distributed and FEM analysis of a mechanical suspended gate, with design guidelines being formulated based on this analysis. Various coupling techniques for impedance mismatch reduction and Q factor enhancement were described and analyzed via equivalent models, and multiphysics FEM and lumped analysis of RSG-FET were carried out in order to estimate the output current of MOSFET and output voltage signal in a common source configuration.

Additionally, RSG-FET-based resonators with various suspended gate lengths were fabricated using the TSMC CMOSP35 process. The post-CMOS release process included RIE CHF3 silicon dioxide etch and aluminum PAN wet etch (for metal sacrificial layers) and RIE SF6 polysilicon etch (for poly2 sacrificial layers). Resonators with 300-400 kHz, 600-800 kHz and 6-7 MHz resonance frequency and Q factor values up to 50 (air) were fabricated and characterized. Due to the relatively low reproducibility of the fabrication process, the resonance frequency and Q factor values had certain deviations. Characterizations with a laser Doppler vibrometer and a lock-in amplifer allowed us to calculate the actual resonance frequency of the devices and their Q factors. The resonance frequency tunability through DC bias and electrothermal actuation was also experimentally investigated and verified in this work.

Bibliography

[1] C. C. Enz and A. Kaiser, *MEMS-based Circuits and Systems for Wireless Communication*. 2013, p. 330.

[2] N. Abelé, K. Séguéni, K. Boucart, F. Casset, B. Legrand, L. Buchaillot, P. Ancey, A. M. Ionescu, and S. T. Microelectronics, "ULTRA -LOW VOLTAGE MEMS RESONATOR BASED ON RSG-MOSFET Gate oxide," no. January, pp. 882–885, 2006.

[3] H. C. Nathanson and R. A. Wickstrom, "A Resonant-Gate Silicon Surface Transistor with High-Q Band-Pass Properties," *Appl. Phys. Lett.*, vol. 7, no. 4, p. 84, 1965.

[4] C. Chin, C. Li, M. Li, and S. Li, "A CMOS-MEMS RESONANT GATE FIELD EFFECT TRANSISTOR," in *Solid-State Sensors, Actuators and Microsystems (TRANSDUCERS & EUROSENSORS XXVII),*, 2013, no. June, pp. 2284–2287.

[5] N. Abele, A. Villaret, A. Gangadharaiah, C. Gabioud, P. Ancey, and A. M. Ionescu, "1T MEMS Memory Based on Suspended Gate MOSFET," in *2006 International Electron Devices Meeting*, 2006, pp. 1–4.

[6] M. Enachescu, A. Van Genderen, and S. Cotofana, "SUSPENDED GATE FIELD EFFECT TRANSISTOR BASED POWER MANAGEMENT - A 32-BIT ADDER CASE STUDY," pp. 561–564.

[7] H. T. S. Aoyagi, M. Suzuki, J. Kogure, T. Kong, R. Taguchi, T. Takahashi, and S. Yokoyama, "ACCELEROMETER USING MOSFET WITH MOVABLE GATE ELECTRODE: ELECTROPLATING THICK NICKEL PROOF MASS ON FLEXIBLE PARYLENE BEAM FOR ENHANCING SENSITIVITY," in *16th International Solid-State Sensors, Actuators and Microsystems Conference*, 2011.

[8] A.-C. Salaun, H. M. Kotb, T. Mohammed-Brahim, F. Le Bihan, H. Lhermite, and F. Bendriaa, "<title>Suspended-gate thin film transistor as highly sensitive humidity sensor</title>," vol. 5836, pp. 231–238, Jul. 2005.

[9] M. I. Younis, *MEMS Linear and Nonlinear Statics and Dynamics*. 2011, p. 456 p.

[10] K. L. Turner, S. A. Miller, P. G. Hartwell, N. C. MacDonald, S. H. Strogatz, and S. G. Adams, "Five parametric resonances in a microelectromechanical system," vol. 396, no. 6707, pp. 149–152, Nov. 1998.

[11] B. DeMartini, J. Moehlis, K. Turner, J. Rhoads, and S. Shaw, “Modeling of Parametrically Excited Microelectromechanical Oscillator Dynamics with Application to Filtering,” in *IEEE Sensors, 2005.*, 2005, pp. 345–348.

[12] D. Dobrescu, L. Dobrescu, A. Rusu, and A. M. Ionescu, “Modeling the suspended gate MOSFET used as voltage programmable switch,” in *2003 International Semiconductor Conference. CAS 2003 Proceedings (IEEE Cat. No.03TH8676)*, 2003, vol. 1, pp. 209–212.

[13] F. Lo Conte, M. Kayal, and A. M. Ionescu, “9 MHz Vibrating Body FET Tuning Fork Oscillator,” pp. 520–523, 2009.

[14] C. Durand, F. Casset, P. Renaux, N. Abele, B. Legrand, D. Renaud, E. Ollier, P. Ancey, A. M. Ionescu, and L. Buchaillot, “In-Plane Silicon-On-Nothing Nanometer-Scale Resonant Suspended Gate MOSFET for In-IC Integration Perspectives,” *IEEE Electron Device Lett.*, vol. 29, no. 5, pp. 494–496, May 2008.

[15] C. C. Enz, F. Krummenacher, and E. A. Vittoz, “An analytical MOS transistor model valid in all regions of operation and dedicated to low-voltage and low-current applications,” *Analog Integr. Circuits Signal Process.*, vol. 8, no. 1, pp. 83–114, Jul. 1995.

[16] Y. S. Chauhan, D. Tsamados, N. Abele, C. Eggimann, M. Declercq, and A. M. Ionescu, “Compact Modeling of Suspended Gate FET,” in *21st International Conference on VLSI Design (VLSID 2008)*, 2008, pp. 119–124.

[17] D. Tsamados, Y. Singh Chauhan, C. Eggimann, K. Akarvardar, H.-S. Philip Wong, and A. Mihai Ionescu, “Finite element analysis and analytical simulations of Suspended Gate-FET for ultra-low power inverters,” *Solid. State. Electron.*, vol. 52, no. 9, pp. 1374–1381, Sep. 2008.

[18] K. Akarvardar, C. Eggimann, D. Tsamados, Y. S. Chauhan, G. C. Wan, A. M. Ionescu, S. Member, R. T. Howe, and H. P. Wong, “Analytical Modeling of the Suspended-Gate FET and Design Insights for Low-Power Logic,” vol. 55, no. 1, pp. 48–59, 2008.

[19] J. F. Rhoads, S. W. Shaw, K. L. Turner, and R. Baskaran, “Tunable Microelectromechanical Filters that Exploit Parametric Resonance,” *J. Vib. Acoust.*, vol. 127, no. 5, p. 423, Oct. 2005.

[20] W. Zhang and K. L. Turner, “Application of parametric resonance amplification in a single-crystal silicon micro-oscillator based mass sensor,” *Sensors Actuators A Phys.*, vol. 122, no. 1, pp. 23–30, Jul. 2005.

[21] B. E. DeMartini, J. F. Rhoads, K. L. Turner, S. W. Shaw, and J. Moehlis, “Linear and Nonlinear Tuning of Parametrically Excited MEMS Oscillators,” *J. Microelectromechanical Syst.*, vol. 16, no. 2, pp. 310–318, Apr. 2007.

[22] H. C. Nathanson, W. E. Newell, R. A. Wickstrom, and J. R. Davis, “The resonant gate transistor,” *IEEE Trans. Electron Devices*, vol. 14, no. 3, pp. 117–133, Mar. 1967.

[23] A. M. Ionescu, V. Pott, R. Fritschi, K. Banerjee, M. J. Declercq, P. Renaud, C. Hibert, P. Fluckiger, and G. A. Racine, “Modeling and design of a low-voltage SOI suspended-gate MOSFET (SG-MOSFET) with a metal-over-gate architecture,” in *Proceedings International Symposium on Quality Electronic Design*, 2002, pp. 496–501.

[24] N. Abele, R. Fritschi, K. Boucart, F. Casset, P. Ancey, and A. M. Ionescu, “Suspended-Gate MOSFET: bringing new MEMS functionality into solid-state MOS transistor,” vol. 00, no. c, pp. 8–10, 2005.

[25] E. K. Chan and R. W. Dutton, “Electrostatic micromechanical actuator with extended range of travel,” *J. Microelectromechanical Syst.*, vol. 9, no. 3, pp. 321–328, Sep. 2000.

[26] N. Abel, “Design and Fabrication of Suspended-Gate MOSFETs for MEMS Resonator , Switch and Memory Applications,” vol. 3838, 2007.

[27] F. M. Alsaleem, M. I. Younis, and L. Ruzziconi, “An Experimental and Theoretical Investigation of Dynamic Pull-In in MEMS Resonators Actuated Electrostatically,” *J. Microelectromechanical Syst.*, vol. 19, no. 4, pp. 794–806, Aug. 2010.

[28] S. A. Bhave, R. T. Howe, B. Sensor, and C. Hall, “INTERNAL ELECTROSTATIC TRANSDUCTION FOR BULK-MODE MEMS RESONATORS,” pp. 59–60, 2004.

[29] H. Chandrahalim, D. Weinstein, L. F. Cheow, S. A. Bhave, O. Group, and P. Hall, “CHANNEL-SELECT MICROMECHANICAL FILTERS USING HIGH-DIELECTRICALLY TRANSDUCED MEMS RESONATORS,” no. January, pp. 894–897, 2006.

[30] D. Weinstein and S. a. Bhave, “Internal Dielectric Transduction of a 4.5 GHz Silicon Bar Resonator,” *2007 IEEE Int. Electron Devices Meet.*, pp. 415–418, 2007.

[31] D. Weinstein and S. A. Bhave, “ACOUSTIC RESONANCE IN AN INDEPENDENT-GATE FINFET,” pp. 2–5, 2010.

[32] D. Weinstein and S. a Bhave, “The resonant body transistor.,” *Nano Lett.*, vol. 10, no. 4, pp. 1234–7, Apr. 2010.

[33] W. Wang, L. C. Popa, R. Marathe, and D. Weinstein, “An unreleased mm-wave Resonant Body Transistor,” *2011 IEEE 24th Int. Conf. Micro Electro Mech. Syst.*, pp. 1341–1344, Jan. 2011.

[34] E. Hwang, S. Member, S. A. Bhave, and S. Member, “Transduction of High-Frequency Micromechanical Resonators Using Depletion Forces in p-n Diodes,” vol. 58, no. 8, pp. 2770–2776, 2011.

[35] E. Hwang, A. Driscoll, and S. A. Bhave, “Platform for JFET-based sensing of RF MEMS resonators in CMOS technology,” *2011 Int. Electron Devices Meet.*, vol. 1, pp. 20.4.1–20.4.4, Dec. 2011.

[36] M. U. Demirci and C. T.-C. Nguyen, “Mechanically Corner-Coupled Square Microresonator Array for Reduced Series Motional Resistance,” *J. Microelectromechanical Syst.*, vol. 15, no. 6, pp. 1419–1436, Dec. 2006.

[37] L. Grasser, H. Mathias, F. Parrain, X. Le Roux, and J. Gilles, “Mems Q-Factor Enhancement Using Parametric Amplification: Theoretical Study and Design of a Parametric Device.” *DTIP of MEMS and MOEMS*, Apr. 2007